HHS Public Access

Author manuscript

Mol Cell. Author manuscript; available in PMC 2022 February 04.

Published in final edited form as:

Mol Cell. 2021 February 04; 81(3): 530–545.e5. doi:10.1016/j.molcel.2020.12.005.

Definition of a Small Core Transcriptional Circuit Regulated by AML1-ETO

Kristy R. Stengel[1,#], **Jacob D. Ellis**[1], **Clare L. Spielman**[1], **Monica L. Bomber**[1], **Scott W. Hiebert**[1,2,a,#]

[1]Department of Biochemistry, Vanderbilt University School of Medicine, Nashville, Tennessee 37232, USA

[2]Vanderbilt-Ingram Cancer Center, Vanderbilt University School of Medicine, Nashville, Tennessee 37232, USA

Summary

Transcription factors regulate gene networks controlling normal hematopoiesis and are frequently deregulated in acute myeloid leukemia (AML). Critical to our understanding of the mechanism of cellular transformation by oncogenic transcription factors is the ability to define their direct gene targets. However, gene network cascades can change within minutes to hours, making it difficult to distinguish direct from secondary or compensatory transcriptional changes by traditional methodologies. To overcome this limitation, we devised cell models in which the AML1-ETO protein could be quickly degraded upon addition of a small molecule. The rapid kinetics of AML1-ETO removal, when combined with analysis of transcriptional output by nascent transcript analysis and genome-wide AML1-ETO binding by CUT&RUN, enabled the identification of direct gene targets that constitute a core AML1-ETO regulatory network. Moreover, de-repression of this gene network was associated with RUNX1 DNA binding and triggered a transcription cascade ultimately resulting in myeloid differentiation.

eTOC Blurb

Stengel et al. combine PROTAC-mediated degradation of the oncogenic transcription factor, AML1-ETO, with nascent transcript analysis to identify direct gene targets. AML1-ETO-mediated repression of this small gene network impairs myeloid differentiation. This provides a model for the identification of transcriptional circuits directly controlled by transcription factors.

Graphical Abstract

[#] To whom correspondence should be sent: VICC, 512 Preston Research Building, 2220 Pierce Ave., Nashville Tennessee, 37232; kristy.r.stengel@vanderbilt.edu; scott.hiebert@vanderbilt.edu, Phone: (615) 936-3582.

[a]Lead contact

Author Contributions

Conceptualization, K.R.S. and S.W.H; Methodology, K.R.S. and S.W.H.; Investigation, K.R.S., J.D.E, C.L.S., M.L.B., S.W.H.; Formal Analysis, M.L.B., C.L.S., K.R.S.; Writing-Original Draft, K.R.S. and S.W.H.; Writing-Review & Editing, K.R.S., J.D.E, C.L.S., M.L.B., and S.W.H.; Visualization, K.R.S. and S.W.H.; Supervision, K.R.S. and S.W.H.; Funding Acquisition, S.W.H.

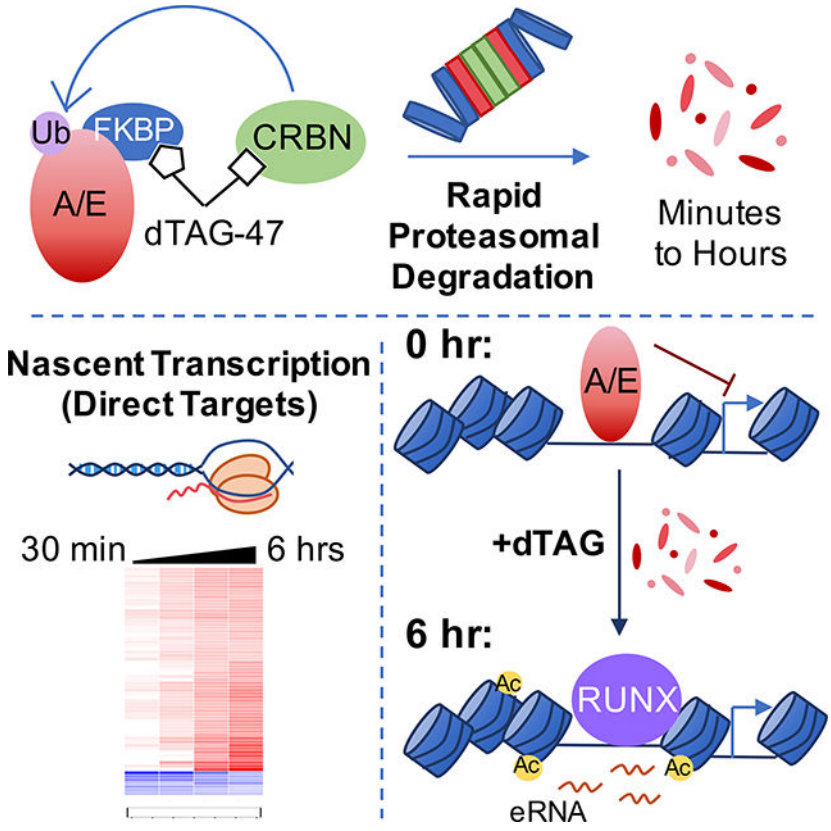

Keywords

myeloid leukemia; AML1-ETO PROTAC; PRO-seq; degron tag; nascent transcription

Introduction

Transcription factors are critical regulators of cell fate decisions and frequent targets of mutations and chromosomal alterations in a variety of human malignancies (Crans and Sakamoto, 2001; Perry et al., 2019). Given the importance of oncogenic transcription factors to the development and progression of human disease (Lee and Young, 2013), the ability to accurately define their direct gene targets is required to truly understand the underlying disease mechanisms, as well as uncover new opportunities for therapeutic intervention. While efforts to define direct transcriptional networks have been underway for decades, the confluence of recent technological advances such as genome editing (Hsu et al., 2014), targeted protein degradation (Roth et al., 2019), and nascent transcript analyses (Wissink et al., 2019) have left us poised to define the true functions of these critical oncogenes.

Traditionally, studies defining gene networks have relied on genetic inactivation of a transcription factor, either through gene deletion or RNAi approaches, followed by measurement of subsequent changes in steady-state mRNA levels. However, these approaches are limited in multiple ways (Muhar et al., 2018). First, the time required for genetic inactivation can take days, thus making it impossible to distinguish direct from

indirect transcriptional events. Second, large differences in mRNA half-lives due to distinct post-transcriptional regulatory mechanisms can further cloud interpretations. These issues have been ameliorated to some degree by correlating the changes in gene expression with genome-wide factor localization methods such as ChIP-seq or CUT&RUN. However, DNA binding is not a good predictor of regulatory activity on nearby genes, and existing data sets often predict binding at many more loci than could feasibly be regulated by a single factor. We combined a chemical-genetic approach for rapid and targeted transcription factor degradation with precision nuclear run-on sequencing (PRO-seq) (Mahat et al., 2016) to directly monitor gene transcription at early timepoints and identify direct gene targets by eliminating the noise created by secondary transcriptional events. Here, we apply this methodology to the analysis of the t(8;21) fusion protein, AML1-ETO (RUNX1-RUNX1T1).

The t(8;21) chromosomal translocation is the single most frequent translocation in acute myeloid leukemia (AML) (Peterson and Zhang, 2004). The AML1-ETO protein includes the DNA binding domain of the RUNX1 (AML1) transcription factor fused to almost the entirety of the ETO (RUNX1T1) transcriptional co-repressor (Erickson et al., 1992; Miyoshi et al., 1993; Miyoshi et al., 1991). Previous studies have sought to define the core AML1-ETO transcriptional program, which underlies its role in myeloid differentiation control (Loke et al., 2017; Ptasinska et al., 2014). However, transcriptional changes were assessed days after knockdown of AML1-ETO expression, which led to the suggestion that AML1-ETO regulates hundreds to thousands of genes, many of which almost certainly represent secondary or compensatory changes in gene expression (Ptasinska et al., 2019). Furthermore, while many existing studies indicate that AML1-ETO functions to repress the expression of critical RUNX1 target genes, numerous studies have also reported that AML1-ETO activates gene expression (Berg et al., 2008; Chen et al., 2015; Li et al., 2006; Li et al., 2016; Martinez-Soria et al., 2018b; Wang et al., 2011). Such seemingly conflicting studies suggest context-specific AML1-ETO functions in transcriptional control, but also highlight the need for experimental approaches that unambiguously define direct transcriptional targets.

We utilized CRISPR-based genome editing to engineer the endogenous *AML1-ETO* locus to create a C-terminal fusion with the $FKBP12^{F36V}$ degron tag (Nabet et al., 2018; Weintraub et al., 2017). This allowed rapid degradation of the endogenous AML1-ETO fusion protein within 30 min to 2hr of treatment with the dTAG-47 proteolysis targeting chimera (PROTAC) (Nabet et al., 2018). Using nascent transcript analysis, we defined a surprisingly small core network of roughly 60 direct AML1-ETO-regulated genes. This network included critical mediators of myeloid differentiation and cell fate decisions such as the transcriptional regulators *CEBPA*, *PLZF* (*ZBTB16*), *NFE2* and *MTG16* (*ETO2* or *CBFA2T3*). Moreover, almost all AML1-ETO-controlled genes were up-regulated immediately following AML1-ETO degradation, suggesting that the fusion protein functions primarily as a transcriptional repressor, rather than to maintain or activate gene expression.

Results

CRISPR-mediated “dTAGging” of endogenous AML1-ETO

Degron tags can rapidly remove transcription factors to identify the direct changes in gene expression and thereby define the underlying molecular mechanisms of action. The kinetics of this approach allow measurements to be taken before compensatory or secondary effects in transcription networks occur. We used CRISPR/Cas9 to insert the FK506 binding protein, *FKBP12*^{F36V}, just prior to the stop codon in the endogenous allele of *AML1-ETO* in the Kasumi-1 t(8;21) cell line (Fig. 1A). This created a protein containing AML1-ETO fused to FKBP12^{F36V} along with a double HA epitope tag. Successfully edited Kasumi-1 cells were isolated by fluorescent activated cell sorting (FACS) using co-expressed mCherry (Weintraub et al., 2017). Western blot analysis detected a mobility shift consistent with the addition of FKPB12^{F36V}, and this more slowly migrating AML1-ETO was also recognized by α-HA (Fig. 1B). As expected, the FKBP12^{F36V} tag rendered AML1-ETO sensitive to the heterobifunctional molecule, dTAG-47 (Weintraub et al., 2017), which bridges FKBP12^{F36V} to the Cereblon E3 ubiquitin ligase (CRBN; Nabet et al., 2018). Treatment of Kasumi-1 *AML1-ETO-FKBP12*^{F36V} cells with 500 nM dTAG-47 caused rapid AML1-ETO degradation, with the majority of the protein eliminated within the first 1–2hr (Fig. 1C). Moreover, this effect appeared specific to AML1-ETO, as the CRBN target, IKAROS (Kronke et al., 2014; Lu et al., 2014), was unaffected (Supplemental Fig. 1A).

Previous studies reported that shRNAs targeting ETO modestly inhibit the growth of t(8;21)-containing Kasumi-1 and SKNO-1 cells (Martinez-Soria et al., 2018b; Schoenherr et al., 2019; Spirin et al., 2014). We found that targeted removal of the fusion protein from Kasumi-1 cells had little effect on cell growth (Fig. 1D) or colony formation/replating assays in methylcellulose (Fig. 1E). However, degradation of AML1-ETO caused loss of CD34^{+} cells (CD34+/CD38+; Fig. 1F), which suggested that the fusion protein was regulating differentiation rather than cell growth and/or viability. The AML1-ETO degradation observed upon dTAG-47 treatment was quite durable, as protein levels did not rebound until 6 days after washout of the small molecule (Fig. 1G). However, the re-expression of AML1-ETO-FKBP12^{F36V} following dTAG-47 washout, did not allow CD34^{+} cells to return to normal levels (Fig. 1H–I).

Defining the core AML1-ETO transcription signature

The tight window of AML1-ETO protein degradation allowed the assessment of early timepoints in order to detect the direct targets of AML1-ETO transcriptional control. Therefore, we performed RNA-seq at short intervals after dTAG-47 treatment. We first compared the gene expression profiles of cells expressing wild-type AML1-ETO with our AML1-ETO-FKBP12^{F36V}-expressing cell line to identify the changes associated with the process of selecting these cells. Using a 1.5-fold cutoff, the RNA-seq analysis showed largely similar gene expression patterns (Supplemental Fig. 1B) with less than 5% of genes varying between the cell lines (Supplemental Fig. 1C), and these variations in gene expression were far fewer than those observed upon degradation of AML1-ETO-FKBP12^{F36V} (Supplemental Fig. 1D).

Further RNA-seq analysis upon AML1-ETO degradation showed a wave of changes in the steady state mRNA pools beginning 2hr after addition of dTAG-47, and by 4hr distinct changes were apparent (Fig. 2A). By 8hr after addition of dTAG-47, some of the genes activated at 2hr and 4hr were already beginning to wane, and new sets of genes were activated. A similar trend was observed at 24hr, with the genes most intensely activated at this late time point having shown minimal activation at 2–4hr. It is also important to note that even though AML1-ETO is commonly regarded as a transcriptional repressor, it has been reported to activate many genes (Berg et al., 2008; Chen et al., 2015; Li et al., 2006; Li et al., 2016; Martinez-Soria et al., 2018b; Wang et al., 2011). Consistent with these reports, our RNA-seq data identified roughly as many mRNAs that decreased as increased upon AML1-ETO degradation (Fig. 2B).

Precision nuclear run-on sequencing (PRO-seq) has been effectively employed at short intervals after treatment with small molecules such as BET inhibitors (Zhao et al., 2016), CDK9 inhibitors (Jonkers et al., 2014), and CDK7 inhibitors (Sampathi et al., 2019) to discern mechanism of action. An advantage of PRO-seq over RNA-seq is that by examining nascent transcripts rather than steady-state mRNA pools, changes in polymerase dynamics can be detected within 15–30 min of the addition of many compounds that target transcription (Sampathi et al., 2019; Zhao et al., 2016). Unlike RNA-seq, which identified a roughly equal number of genes repressed as activated upon AML1-ETO degradation (Fig 2B), PRO-seq detected a small but stable number of genes showing reduced expression between 30 min and 6hr, whereas it detected a steady increase in the number of genes that became activated over time (Fig. 2C). This is consistent with a more prominent role for AML1-ETO in transcriptional repression. Moreover, when we examine the identity of genes that were down-regulated at each time point following dTAG-47 treatment, we observed very little overlap, with only 7 genes consistently down-regulated at 1, 2, and 6hr (Fig. 2D, right panel). By contrast, the 13 genes that were induced at least 1.5-fold (using a 50 bp sliding window across the gene body, $q < 0.05$ (Liu et al., 2017; Wang et al., 2018)) at 1hr post-treatment became more robustly induced at 2hr, and 59 genes induced at 2hr remained induced at 6hr (Fig. 2C, 2D left panel). A heat map depicting the 59 genes with increased expression and 7 genes with decreased expression (Fig. 2E) revealed a steady increase in expression over time of the former, whereas the decreased genes were trending back to their starting transcriptional states by 6hr (Fig. 2E).

Of note, the canonical AML1-ETO-regulated genes *CEBPA*, *CD82*, and *ETO2* (Fig. 2E) were induced at least 1.5-fold within 2hr (FDR-adjusted p value: $q < 0.05$). Gene tracks showing transcriptionally engaged polymerase across the *ZBTB16* (*PLZF*) and *GPR114* loci show an observable increase in transcription by 1hr, with even more dramatic increases observed by 6hr following dTAG-47 treatment (Fig. 2F, 2G). Because key transcriptional regulators like *CEBPA, NFE2, ZBTB16*, and *ETO2* were already induced within 2hr of dTAG-47 addition, we reasoned that changes in transcription at 6hr could be indirect. Therefore, we defined the 59 genes altered within 2hr of dTAG-47 treatment as a high-confidence AML1-ETO repression signature.

We also intersected the PRO-seq and RNA-seq data, which showed that by 4–8hr the RNA-seq analysis had captured the same gene signature as the PRO-seq analysis, but also

identified a number of changes in steady state transcripts that lacked a clear transcriptional basis (Supplemental Fig. 1E and 1F). Accordingly, we noted that *CEBPA* levels began to decline 24hr after treatment in the RNA-seq analysis, while *CEBPE* transcription increased (Supplemental Fig. 1G), which is typical of myeloid differentiation transcriptional cascades. These results further highlight the need for the analysis of short time courses using assays measuring nascent transcription in order to identify direct transcriptional changes.

PRO-seq maps all transcriptionally engaged RNA polymerase, therefore, it yields mechanistic transcriptional data including changes in polymerase pausing and elongation (Supplemental Fig. 2A). Heatmaps and histograms constructed around the transcritional start sites of genes identified as significantly activated or repressed based on gene body changes in polymerase density showed no effects on RNA polymerase pausing following the degradation of AML1-ETO (Supplemental Fig. 2B, 2C). Rather both promoter proximal and gene body polymerase levels appeared elevated in activated genes. However, direct quantification of promoter proximal polymerase levels and calculation of pausing index revealed that the most significant effect of AML1-ETO degradation on gene expression was an increase in gene body polymerase (Supplemental Fig. 2D–H).

Functional annotation of AML1-ETO binding sites

Given that the targeted degradation of AML1-ETO identified a much smaller core transcriptional signature as compared to genetic deletion or RNAi approaches, we performed CUT&RUN analysis to determine if the FKBP12^{F36V}-2xHA tag had altered AML1-ETO target selection. Because CUT&RUN does not use formaldehyde crosslinking, this also provides an analysis of native DNA binding by the endogenous fusion protein. This approach identified over 30,000 peaks that were significantly decreased upon degradation of the fusion protein (Fig. 3A, Supplemental Fig. 3A and 3B). Most peaks identified by α-HA CUT&RUN were lost upon dTAG-47 treatment, confirming the specificity of this analysis. Critically, the vast majority of these peaks overlapped with previous ChIP-seq data (Trombly et al., 2015), as well as CUT&RUN performed on parental Kasumi-1 cells using an α-ETO antibody to detect wild-type AML1-ETO binding (Supplemental Fig. 3A and 3B). Thus, wild-type AML1-ETO and AML1-ETO-FKBP12^{F36V}-2xHA (α-HA) genome binding were highly consistent, both with one another and with previously published AML1-ETO ChIP-seq data sets. Importantly, all 59 genes that were activated in the first 2hr of dTAG-47 treatment (Fig. 2) displayed robust AML1-ETO binding. K-means clustering segregated the AML1-ETO-FKBP-HA peaks into three clusters based on signal intensity (Fig. 3A) and the AML1-ETO peaks within clusters 1 and 2 showed an even split between promoter and enhancer (intronic and intergenic) binding, while cluster 3 consisted of predominantly intronic and intergenic peaks (Fig. 3B). All three clusters contained some sites associated with the 59 gene repression signature (Supplemental Fig. 3C) and were enriched for RUNX and ETS binding motifs (Supplemental Fig. 3D).

To functionally characterize AML1-ETO binding sites, we performed ChIP-seq for H3K27ac, a mark of active enhancers and promoters, before and after degradation of AML1-ETO. By plotting the H3K27ac signal around all AML1-ETO peaks, even when separated into clusters 1–3, we found minimal global changes in H3K27ac following AML1-ETO

degradation (Fig. 3C). In fact, the H3K27ac signal was slightly decreased at total AML1-ETO bound sites following dTAG-47 treatment (Fig. 3C, upper). In contrast, based on nearest gene annotation, the most intense AML1-ETO peaks (clusters 1 and 2, Fig. 3A) that were associated with the 59 gene repression signature identified by PRO-seq, showed a robust increase in H3K27ac upon AML1-ETO-degradation (Fig. 3C, lower). Thus, the major changes in acetylation occurred at sites with high levels of AML1-ETO occupancy and associated with the 59 gene repression signature.

Like gene promoters, active enhancers are characterized by bi-directional transcription inititaion (Henriques et al., 2018). Therefore, we also plotted the PRO-seq signal +/− 2,000 bp around identified AML1-ETO-binding sites. Much like H3K27ac, there was no change in active polymerase around AML1-ETO binding sites when all peaks were included in the analysis (Fig. 3D, upper). However, when we focused on peaks associated with the 59 gene repression signature, we observed an increase in nascent transcription just 2hr after dTAG-47 addition (Fig. 3D, lower). Thus, it appears that functional AML1-ETO peaks were enriched in clusters 1 and 2, and are characterized by both an increase in H3K27ac and active RNA polymerase following AML1-ETO degradation.

Given the robust changes in enhancer and promoter activity within 2hr of dTAG-47 addition, we performed a time course analysis for H3K27ac (Fig. 3E). In addition, we assessed H3K4me3 levels 24hr after dTAG-47 treatment (Fig. 3F). H3K27ac at the 59 gene signature showed an early and sustained increase (Fig. 3G, left). In contrast, H3K4me3 levels were increased 24hr after dTAG-47 addition, and while the change in this histone mark was similar whether assessing all peaks or those associated with the 59 gene signature, the baseline H3K4me3 level was dramatically reduced at AML1-ETO-binding sites associated with the 59 gene repression signature compared with all AML1-ETO peaks, suggesting AML1-ETO-mediated suppression of this mark (Fig. 3G, right). In addition, depiction of the H3K4me3 signal around the transcription start site of regulated genes showed a more dramatic increase in signal following AML1-ETO degradation (Supplemental Fig. 4A). These molecular events become even clearer when analyzing the individual dynamics of members of the core 59 gene signature. For instance, the *CD82* locus is characterized by an intronic enhancer, which exhibits a prominent AML1-ETO peak that was subsequently lost following dTAG treatment (arrow, Fig. 3H). The enhancer displayed a rapid increase in H3K27ac, an increase in H3K4me3, and an increase in active polymerase within 2hr of AML1-ETO degradation (Fig. 3H). Moreover, these changes were associated with an observeable increase in *CD82* gene transcription by 1hr that became even more significant by 6hr (Fig. 3H). Thus, AML1-ETO peaks associated with functional gene repression were characterized by a low level of H3K4me3, and exhibited a rapid increase in H3K27ac and active polymerase upon AML1-ETO degradation.

Given that the majority of the AML1-ETO binding sites could not be easily linked to changes in gene expression, we tested whether these loci were more stably silenced by the Polycomb-placed repressive mark, H3K27me3. CUT&RUN using α-H3K27me3 was performed before and after dTAG-47 treament (Supplemental Fig. 4B), and the H3K27me3 peaks were associated with over 5500 genes. Roughly 20% of the genes associated with an AML1-ETO peak were also marked by H3K27me3 (Supplemental Fig. 4C). Moreover, the

degradation of AML1-ETO was not suffient to remove this repressive mark (Supplemental Fig. 4A and 4B), suggesting that the chromatin context of AML1-ETO binding sites may hamper the activation of some genes following AML1-ETO degradation.

RUNX1 replaces AML1-ETO at select sites after fusion protein degradation

We next performed motif analysis specifically on AML1-ETO peaks associated with the 59 repressed genes to determine if these regions were enriched in other transcription factor binding sequences. We found that, as with the analysis of total AML1-ETO peaks (Supplemental Fig. 3D), these peaks were overwhelmingly enriched for RUNX and PU.1 motifs (Fig. 4A), which is consistent with RUNX family members cooperatively binding DNA with ETS factors (Martens et al., 2012; Trombly et al., 2015). Somewhat surprisingly, E protein binding sites were not among the top five results of the motif analysis (Fig. 4A), even though they displayed robust binding to AML1-ETO (Sun et al., 2013; Zhang et al., 2004).

We used CUT&RUN to assess the genomic localization of both RUNX1 and PU.1 before and after degradation of AML1-ETO (Fig. 4B–D). This analysis identified in excess of 30,000 peaks for both factors with most of these peaks overlapping with the peaks from the α-HA-AML1-ETO dataset (Fig. 4C). Surprisingly, very few of the RUNX1 peaks were significantly increased 6hr after AML1-ETO degradation (Fig. 4B, red dots in the center and right panels and Fig. 4D) and even fewer of the PU.1 peaks reached statistical significance. Notably, the increase in RUNX1 and PU.1 CUT&RUN signal was particularly prominent at peaks associated with the 59 genes that were induced upon AML1-ETO degradation (Fig. 4E&F, lower). These changes in specific peaks become more clear when analyzing individual peaks within members of the core 59 gene signature. For instance, while *CBFA2T3 (ETO2)* and *CEBPA* showed multiple AML1-ETO peaks that were lost upon dTAG treatment, only select peaks were characterized by both a reduction in AML1-ETO, increased RUNX1, and to a lesser degree, increased PU.1 occupancy. Moreover, it is specifically these peaks that show an increase in H3K27ac within 2hr of dTAG-47 treatment (blue arrows, Fig. 4G and H).

The NH4 domain is required for repression by AML1-ETO

As a further functional test of the AML1-ETO-FKBP12^{F36V} allele, we expressed wild type or mutant forms of AML1-ETO in our AML1-ETO-FKBP12^{F36V} cells and then degraded the endogenous fusion protein to test for complementation. The cell surface marker, *CD82*, is one of the most highly up-regulated target genes (Fig. 3H), and FACS analysis for this cell surface protein yielded easily quantifiable results in which CD82 was maximally induced within 24hr of AML1-ETO-FKBP12^{F36V} degradation (Fig. 5A). Thus, we were able to use CD82 expression as a biomarker of AML1-ETOmediated gene repression. Unexpectedly, a mutant that disrupted the ability of ETO to repress HEB or E2A-mediated transactivation (AML1-ETO^{F332A}) (Hunt et al., 2011; Plevin et al., 2006) or deletion of the entire NH1 domain had essentially no impact on *CD82* repression (Fig. 5B–E). By contrast, ΔNH4, which appears to suppress leukemia development in mice (Yan et al., 2006), was unable to fully repress *CD82* (Fig. 5D), and three point mutations within NH4 (R668H, G676C, or W692A) had varying effects on AML1-ETO-mediated repression (Fig. 5E). NH4 is

responsible for one of the two contacts between NCOR1/SMRT, with a second contact site lying between NH1 and NH2 of ETO that alone is sufficient for co-immunoprecipitation of NCOR1 with AML1-ETO (Amann et al., 2001; Gelmetti et al., 1998; Lutterbach et al., 1998a; Lutterbach et al., 1998b; Wang et al., 1998). Deletion of both the second NCOR1 binding domain and NH4 completely eliminated AML1-ETO-mediated repression of *CD82* (Fig. 5D).

Rapid loss of self-renewal and differentiation upon degradation of AML1-ETO in long-term CD34$^+$ HSPC cultures

The relatively modest effects on the growth of Kasumi-1 cells upon degradation of AML1-ETO or knockdown of AML1-ETO using shRNAs (Martinez-Soria et al., 2018b; Schoenherr et al., 2019; Spirin et al., 2014), suggested that these cells may have sustained other mutations or epigenetic changes that allowed them to continue to proliferate in the absence of AML1-ETO, albeit with some differentiation (Fig. 1). In fact, Kasumi-1 cells contain both mutations associated with relapse (e.g., *KIT* (Ayatollahi et al., 2017)), as well as mutations rarely observed in t(8;21) patients (e.g. *TP53* (Hou et al., 2015)). Consequently, we turned to long-term cultures of CD34$^+$ cells from human cord blood to establish a pre-leukemic system to study AML1-ETO transcriptional functions in the absence of potentially confounding mutations. Expression of AML1-ETO in these primary cells impaired myeloid differentiation in the presence of cytokines that promote myelopoiesis (Wunderlich and Mulloy, 2009) and allowed for the establishment of a long-term, pre-leukemic state (Mulloy et al., 2003). We expressed AML1-ETO or AML1-ETO-FKBP12^{F36V} in CD34$^+$ HSPCs and found that the addition of the FKBP12 moiety did not affect the ability of AML1-ETO to induce the long-term growth of CD34+ cells, or to repress the expression of *CD82* (Supplemental Fig. 5A–C). When AML1-ETO-FKBP12^{F36V} was degraded upon addition of dTAG-47 (Fig. 6A), cell growth halted (Fig. 6B), CD34 expression was lost (Fig. 6C), and the cells underwent complete myeloid differentiation as indicated by the expression of CD11B and morphological changes (Fig. 6C–E). In contrast, CD34$^+$ cultures expressing wild-type AML1-ETO were unaffected by dTAG-47 treatment (Supplemental Fig. 5D–F).

Next, we used CUT&RUN to ensure that the exogenously expressed AML1-ETO-FKBP12^{F36V} bound to DNA appropriately (Fig. 6A) and found that the majority of binding sites identified in CD34$^+$ cultures overlapped with the CUT&RUN data from Kasumi-1 cells (Fig. 6F; see examples *RASSF2*, *CD82* and *NFE2* Fig. 6G). Due to limited cell numbers, we used RNA-seq at a short interval (4hr) after addition of dTAG-47 to examine changes in gene expression and this analysis identified 107 genes induced and 9 genes whose expression decreased (Fig. 6H). By comparing these data with the 4hr RNA-seq data from Kasumi-1 cells, we found that 50 of the 107 genes up-regulated in CD34$^+$ cells were induced in both systems (Fig. 6I). While this concordance is high, it likely underestimates the similarities, because the short time frame used for RNA-seq to capture direct changes in the CD34+ cells failed to capture canonical targets such as *CD82, OGG1* and *RASSF2*, which were trending upward but did not reach our statistical cutoff within 4hr (Fig. 6G, I). In fact, CD82 protein levels were significantly up-regulated in CD34$^+$ cultures by 24hr post-dTAG treatment (Fig. 6J). Additionally, we observed changes in the expression of *GFI1B* and key stemness genes such as *MYCN* that were unique to the CD34$^+$ system (Fig. 6I).

GFI1B was the second most highly upregulated gene in $CD34^+$ cells, but was not induced in Kasumi-1 (Fig. 7A). *GFI1B* is particularly intriguing, as it is a RUNX1-regulated gene that is critical for megakaryopoiesis (Anguita et al., 2017; Lancrin et al., 2012). Interestingly, *RUNX1* mutations were observed in familial platelet disorders that predispose these patients to AML development (Jongmans et al., 2010), suggesting that deregulation of RUNX1-mediated *GFI1B* control may contribute to pathogenesis. Given the lack of induction of *GFI1B* and the observation that some AML1-ETO bound genes were marked by H3K27me3 in Kasumi-1 cells, we performed CUT&RUN assays for H3K27me3 to assess this epigenetic mark across the genome in $CD34^+$ HSPCs as well. We found that H3K27me3 marked some loci in common between Kasumi-1 and $CD34^+$, but there were also large differences. One of those differences was *GFI1B*, which showed H3K27me3 throughout the *GFI1B* locus in Kasumi-1 cells, but little H3K27me3 in primary HSPC cultures (Fig. 7C, D). To test if the failure to re-activate *GFI1B* expression upon AML1-ETO degradation in Kasumi-1 cells contributed to the reduced level of differentiation observed in this system, we exogenously expressed Gfi1b in Kasumi-1 cells and then degraded AML1-ETO-$FKBP12^{F36V}$. Exogenous expression of Gfi1b tripled the number of CD11B positive cells observed 9 days after dTAG47 treatment (Fig. 7 F, G).

LSD1 (KDM1A) inhibitors activated *GFI1B* transcription in a variety of cell types, LSD1 was found to co-purify with AML1-ETO (Chen et al., 2015; Johnston et al., 2020; Maiques-Diaz et al., 2018; van Bergen and van der Reijden, 2019), and H3K4me3 was low around AML1-ETO binding sites (Fig. 4E, F). Therefore, we performed CUT&RUN analysis for LSD1 in Kasumi-1 cells, and found that LSD1 peaks showed extensive overlap with AML1-ETO peaks (Fig. 7H), However, these LSD1 peaks did not change upon degradation of AML1-ETO (Fig. 7I), suggesting that AML1-ETO was not required to maintain LSD1 at target loci. For example, within the *GFI1B* locus, there were prominent AML1-ETO peaks at the 5' most promoter (blue arrow, Fig. 7J) and at a downstream enhancer (Fig. 7J, see the expanded panel below). While both AML1-ETO peaks were lost upon degradation of the fusion protein, the LSD1 peaks were unchanged. Treatment of Kasumi-1 cells with both dTAG-47 to degrade AML1-ETO and an LSD1 inhibitor (100 nM GSK2879552) was needed to activate the *GFI1B* enhancer (expanded panel below Fig. 7J), induce *GFI1B* mRNA (Fig. 7K), and trigger differentiation to a level similar degree as Gfi1b overexpression, Supplemental Fig. 6A, Fig. 7G). Further combining dTAG/LSD1i treatment with all trans-retinoic acid (ATRA) resulted in an even more dramatic differentiation of Kasumi-1 cells as monitored by CD11B and morphological cell changes (Fig. 7L, Supplemental Fig. 6A–C). Thus, even in a cell line that contains additional mutations not commonly observed in t(8;21) patients (e.g., mutant *TP53*), understanding the direct targets for repression by AML1-ETO (Fig. 2–6) had important biological and potentially therapeutic effects (Fig. 7).

Discussion

One of the biggest challenges in studying transcription factor function is to define the direct, primary gene targets. The development of modern genomic methods (e.g. ChIP-seq and RNA-seq) coupled with RNAi approaches allows genome-wide analysis. Yet, as we observed, most DNA binding sites can not be assigned a function in terms of transcription or

histone acetylation (e.g., Fig. 3, 4, 6, 7). This is perhaps not surprising for a transcription factor that binds a small consensus site (Melnikova et al., 1993; Meyers et al., 1993; Ogawa et al., 1993), as these analyses yield far more potential binding sites than genes to regulate. Furthermore, waiting two to ten days after gene knockdown before measuring gene expression makes it difficult to deconvolute direct from indirect transcriptional changes (Martinez-Soria et al., 2018b; Ptasinska et al., 2012). Thus, in many cases, the changes in gene expression attributed to loss of a transcription factor were actually a consequence rather than the cause of phenotypic changes observed days after knockdown. Likewise, exogenous expression of AML1-ETO in human embryonic stem cell lines caused phenotypic changes and cell cycle defects, which complicated the interpretation of the genomic analysis (Nafria et al., 2020).

By integrating a small molecule-responsive degron tag into the endogenous locus of AML1-ETO and coupling the rapid degradation of this factor to genome-wide nascent transcription assays, we have established a system to collapse the time frame for transcription factor analysis from days to minutes. This degron approach is agnostic to the effect of AML1-ETO on gene regulation (i.e., repression vs. activation), as we capture events indicative of either possibility using PRO-seq (Jonkers et al., 2014; Mahat et al., 2016). The prior studies that suggested that AML1-ETO was required for gene expression (i.e., activation) used siRNA or shRNAs, and RNA-seq was performed between 48hr and 10 days after transfection or infection. One such study found that AML1-ETO was critical for maintaining *Cyclin D2* (*CCND2*) expression (Martinez-Soria et al., 2018a). However, our data indicated that AML1-ETO degradation did not correlate with either a loss of H3K27ac or active polymerase at the *CCND2* enhancer, and there was no change in the rate of *CCND2* transcription over the PRO-seq time course (Supplemental Fig. 7A–C). These differing results can most easily be explained by differences in experimental kinetics.

The finding that *GFI1B* was reactivated upon AML1-ETO degradation in differentiating pre-leukemic cultures, but not in the t(8;21) cell line demonstrates how mechanistic insights can lead to novel therapeutic strategies. Recent studies have identified GFI1 and GFI1B, two transcription factors that repress their own expression, as the critical targets of LSD1 inhibition (Johnston et al., 2020; Maiques-Diaz et al., 2018; van Bergen and van der Reijden, 2019), leading us to ask whether combining an LSD1 inhibitor with AML1-ETO degradation could reactivate *GFI1B* expression in Kasumi-1 cells. Not only did this combination result in a dramatic increase in *GFI1B* expression, but the combination caused an increase in Kasumi-1 cell differentiation (Fig. 7, Supplemental Fig. 6). Moreover, consistent with previous reports of cooperativity between LSD1 inhibitors and ATRA in AML models (Schenk et al., 2012), the addition of ATRA to the dTAG/LSD1i combination further facilitated the differentiation of Kasumi-1 cells (Supplemental Fig. 6). Given the possible need to reverse H3K27me3, the targeting of t(8;21) AML may require combination therapy to target multiple histone modifying complexes in conjunction with differentiation therapy.

Limitations

A caveat of this work is that it is limited to Kasumi-1 cells and $CD34^+$ primary human stem/progenitor cells expressing *AML1-ETO-FKBP12*^{F36V}. In each instance, there is some selection that occurs in establishing these cell populations. An additional limitation is the imposition of a short time frame to define direct targets for regulation by AML1-ETO. It is possible that other genes are regulated by AML1-ETO, but not reactivated within the first 4–6hr of degradation (e.g., *GFI1B* in Kasumi-1 cells). However, given that many transcription factors were activated within this time frame, this strict time limitation was required to ensure only the identification of direct effects of AML1-ETO-dependent transcriptional control.

STAR Methods

Resource Availability

Lead Contact

Further information and requests for resources and reagents should be directed to and will be fulfilled by the Lead Contact, Scott Hiebert (scott.hiebert@vanderbilt.edu).

Materials Availability—All the materials generated in this study are accessible upon request.

Data and Code Availability—All genomic datasets are available at GEO accession GSE153281. Original data for figures in this study are accessible upon request and deposited to Mendeley Data: https://data.mendeley.com/datasets/3z2g7cs2ht/draft?a=05c22fa8-bd6b-4f3b-9788-c16dc6adfe83

Experimental Model Details

Cell Lines—Kasumi-1 cells were a generous gift of James Mulloy, Cincinnati Children's Hospital and were maintained in RPMI supplemented with 15% FetalPlex, 50 U/ml penicillin, 50 μg/ml streptomycin, and 2mM L-glutamine. The Kasumi-1-AML1-ETO-$FKBP12^{F36V}$ cell line was generated as described in the method details and cultured under the same conditions as parental Kasumi-1 cells. $CD34^+$ human cord blood cells were obtained from StemCell Technologies, and long-term $CD34^+$ HSPC cultures were established by overexpression of AML1-ETO or AML1-ETO-$FKBP12^{F36V}$ using murine stem cell virus (MSCV) (Wunderlich and Mulloy, 2009) and cultured as described in the Method Details.

Method Details

Cell Culture.—$CD34^+$ human cord blood cells were obtained from StemCell Technologies, and long-term $CD34^+$ HSPC cultures were established by overexpression of AML1-ETO or AML1-ETO-$FKBP12^{F36V}$ using murine stem cell virus (MSCV) as previously described (Wunderlich and Mulloy, 2009). Briefly, cells were thawed into pre-stimulation media (IMDM supplemented with 20% FBS, 55 μM BME, 50 U/ml penicillin, 50 μg/ml streptomycin, 2mM L-glutamine, and 100 ng/mL SCF, TPO, and Flt3-L).

Following retroviral transduction, cultures were maintained in a myeloid culture media (IMDM supplemented with 20% FBS, 55 μM BME, 50 U/ml penicillin, 50 μg/ml streptomycin, 2mM L-glutamine, and 10 ng/mL SCF, Flt3-L, TPO, IL-3, and IL-6).

dTAG-47.—dTAG-47 was previously described (Weintraub et al., 2017), and was synthesized by the Vanderbilt University School of Medicine Chemical Synthesis Core. dTAG-47 was reconstituted in DMSO and used throughout the study at a working concentration of 500 nM.

CRISPR-Cas9.—Kasumi-1 cells were engineered to incorporate a C-terminal $FKBP12^{F36V}$-2xHA tag encoded in the endogenous AML1-ETO locus using CRISPR-Cas9-mediated gene editing. Briefly, crRNA targeting the 3' end of *RUNX1T1 (ETO)*-TCTGAGTTCACGTCTAGCGAwas annealed with tracrRNA (IDT). Annealed gRNAs were assembled into RNP complexes by incubation with Alt-R S.p. Cas9 Nuclease V3 (IDT) at room temperature. RNP complexes and equimolar HDR plasmid targeting the 3' exon of *RUNX1T1* and containing *$FKBP12^{F36V}$-2xHA-P2A-mCherry* were electroporated into Kasumi-1 cells. Successfully edited cells were sorted based on mCherry expression no sooner than 7 days following electroporation.

Retrovirus production/transduction.—Full length *AML1-ETO* was cloned into the *MSCV-IRES-GFP* retroviral expression vector. The indicated domain deletions and point mutations were generated by site-directed mutagenesis using the QuickChange Lightning Site-Directed Mutagenesis kit (Agilent). The Gfi1b expression plasmid, pcDNA3.1-Gfi1b-Flag was a generous gift from H. Leighton Grimes, Cincinnati Children's Hospital Medical Center. *Gfi1b-Flag* was cloned into *MSCV-IRES-GFP* by Gibson assembly (NEB). For $CD34^+$ HSPC cultures, *AML1-ETO-$FKBP12^{F36V}$-2xHA* or wild-type *AML1-ETO* were cloned into the *MSCV-IRES-mCherry* vector. For virus production, MSCV-based retroviral vectors, plus pCMV5 expressing a cDNA encoding the vesicular stomatitis virus G protein, plus the *pMD-gag-pol* plasmid were transfected into 293T cells with polyethylenimine. For infection of Kasumi-1 cells, 48 hr post-transfection, viral supernatant was filtered and spun onto cells in the presence of 8μg/mL polybrene. For infection of $CD34^+$ cord blood cells, filtered viral supernatant was spun onto a retronectin-coated dish, cells were added to virus-coated plates in the presence of 8μg/mL polybrene and incubated in the presence of virus overnight at 37°C. Infected cells were washed the following day and placed in fresh media.

Western Blotting.—Cells were lysed in RIPA buffer supplemented with protease inhibitors and sonicated to shear DNA. Cleared lysates were resolved by SDS-PAGE, transferred to PVDF membrane and probed with specified antibodies. *Antibodies: α*-HA – Abcam ab18181, α-Lamin B- Santa Cruz sc-6217, α-IKAROS Santa Cruz sc-398265, α-GAPDH Santa Cruzsc-365062, α-Runx Homology Domain (RHD) made in house.

Flow cytometry.—Cells were washed and resuspended at a concentration of 1 million cells per 100 μl in PBS + 0.5% BSA. Cells were stained with the indicated antibodies at the manufacturer's suggested concentration for 20 minutes at 4°C, washed and acquired using a BD 4 Laser Fortessa flow cytometer. *Antibodies*: CD82 (BD, clone 423524), CD11b (BD, clone ICRF44), CD34 (BD, clone 581), CD38 (BD, clone HIT2).

Q-RT-PCR.—Kasumi-1 AML1-ETO-FKBP cells were treated for 3 days with 500 nM dTAG-47 alone, 100 nM LSD1i (GSK2879552, Selleckchem, S7796) alone, dTAG and LSD1i, or dTAG, LSD1i and 1 μM ATRA (Sigma-Aldrich, R2625). Total RNA was isolated by Trizol extraction according to the manufacturer's protocol. 2 μg of RNA was used for reverse transcription (High Capacity cDNA Reverse Transcription Kit, ThermoFisher). Quantitative PCR detecting *Gfi1b* and *Actb* was carried out using SYBR green master mix (Bio-Rad). PCR primers: *Gfi1b* F- AGAAGGCTCACACCTACCAC, *Gfi1b* R-GCTAGGCTTGTAGAATGGGGG *Actb* F- ACCTTCTACAATGAGCTGCG, *Actb* R-CCTGGATAGCAACGTACATGG.

Methylcellulose assays.—Kasumi-1-AML1-ETO-wild-type or Kasumi-1-AML1-ETO-FKBP cells were treated for 24 hr with 500 nM dTAG-47 prior to plating in methylcellulose (MethoCult H4434, StemCell Technologies). 500 cells were plated in 1.1 mL Methocult supplemented with 500 nM dTAG-47. Colonies were counted 12 days after plating, cells harvested and re-plated in Methocult with fresh dTAG molecule.

RNA-seq.—All RNA-seq experiments were performed in biological replicates. Total cellular RNA was isolated using Trizol Reagent (Invitrogen) according to the manufacturer's protocol. 5 μg of RNA was subject to DNase digestion, phenol-choloroform extracted and ethanol precipitated. RNA was submitted to Vanderbilt University Medical Center VANTAGE Core for poly-A enrichment-based library preparation and sequencing on the Illumina NovaSeq (PE-100). *Data Analysis.* Pre-processed reads were aligned to the human genome (hg19, downloaded from UCSC) using TopHat (v2.0.11) and differential gene expression was determined using Cuffdiff (v.2.1.1) as previously described (Trapnell et al., 2013).

PRO-seq.—All PRO-seq experiments were performed in biological replicates. Nuclear run-on and PRO-Seq library construction were performed as previously described (Zhao et al., 2016), with *in vitro* transcribed and biotinylated *Luciferase*, *GFP*, and *NeoR* transcripts included as spike-in controls. Briefly, cells were treated with 500 nM dTAG-47 for 30 min, 1 hr, 2 hr, 6 hr or treated with 500 nM dTAG-47 alone, 100 nM GSK2879552 alone or dTAG + GSK2879552 for 24 hr prior to nuclei isolation. 30×10^6 nuclei were used per run-on. Nuclear run-ons were carried out in the presence of 375 μM of biotin-11-CTP, ATP, UTP and GTP and 0.5% sarkosyl for 3 minutes at 30°C. Total RNA was hydrolyzed with 0.2N NaOH and nascent RNAs that had incorporated biotin-11-CTP were isolated by streptavidin bead binding. Libraries were prepared using custom reagents as previously described (Zhao et al., 2016) and were PAGE purified and provided to Vanderbilt University Medical Center VANTAGE Core for sequencing on an Illumina Nextseq 500 (SR-75). *Data Analysis.* Adaptors were trimmed and reads shorter than 15 bp were removed using Trimmomatic-0.32 (Bolger et al., 2014). Reverse complement sequences were obtained using FASTX toolkit (v 0.0.13) prior to aligning to the human genome (hg19) using Bowtie2 (v2.2.2) (Langmead and Salzberg, 2012). Analysis of PRO-seq data was carried out using the Nascent RNA Sequencing Analysis (NRSA) pipeline (Wang et al., 2018).

CUT&RUN.—A-HA (Cell Signaling Technology, C29F4), α-ETO (made in house), α-H3K4me3 (Abcam, mAbcam12209), α-H3K27me3 (Cell Signaling Technology, C36B11), α-RUNX1 (Santa Cruz, A-2), α-PU.1 (Santa Cruz, C-3), and α-LSD1 (Abcam, ab17721) primary antibodies were used for CUT&RUN analysis. A-Rabbit secondary antibody (Invitrogen, 31238) or α-mouse secondary antibody (Abcam, ab46540) were utilized as previously described (Skene et al., 2018). Briefly, 250,000 cells were washed in buffer containing digitonin (0.01% digitonin for Kasumi-1 cells, 0.04% digitonin for $CD34^+$ HSPCs) and bound to 10 μl of activated Concanavalin A beads (Bangs Laboratories Inc., BP531). Bead-bound cells were incubated with α-HA (1:800) overnight, washed, and incubated with α-rabbit secondary (1:100) for 1 hr. For α-ETO, cells were processed in buffer containing 0.02% digitonin and incubated with 10 μg/ml α-ETO without secondary. After washing, cells were incubated with CUTANA pA/G-MNase (Epicypher) and targeted chromatin digestion initiated by the addition of 100 mM $CaCl_2$ and allowed to proceed for 2 hr at 4°C (α-ETO was digested for 30 min at 4°C), at which time stop buffer containing *S. cerevisi* spike-in DNA was added. Released chromatin fragments were purified by phenol-chloroform extraction followed by ethanol precipitation. Libraries were generated using the NEBNext Ultra II DNA Library Prep Kit and sequenced on the Illumina NovaSeq (PE-100) at Vanderbilt University Medical Center VANTAGE core. *Data Analysis.* Adaptors were trimmed with Trimmomatic-0.32 prior to aligning to the hg19 genome with Bowtie2 (v 2.2.2). Spike-in reads were removed and quantified. Peaks were called using MACS2 peak caller (narrowPeak; q-0.001; v 2.0.10.20131216) (Feng et al., 2012). Peaks with significantly lower signal following dTAG treatment were identified with DiffBind (Ross-Innes et al., 2012)and DESeq2 (Love et al., 2014) and subsequent data analysis performed using HOMER (Heinz et al., 2010) and deepTools (v 3.4.3) (Ramirez et al., 2016). Using deeptools, BigWig were generated using the bamCoverage command, matrices were generated by computeMatrix, and utilized for heatmap generation by plotHeatmap.

ChIP-seq.—α-H3K27ac (abcam ab4729) was used for ChIP-seq using on 10 million Kasumi-1 AML1-ETO-FKBP cells at 0- and 24-hr post-treatment with dTAG-47 and with *Drosophila* S2 cell spike-in. Cells were cross-linked with 1% formaldehyde for 10 minutes RT and quenched with 125 mM Glycine. Following cell lysis, chromatin was sonicated with a Biorupter (Diagenode) to generate 300–600 bp chromatin fragments and immunoprecipitated with antibody plus Protein A:G beads. Library construction was carried out using the NEBNext Ultra II DNA Library Prep Kit and sequenced on the Illumina NovaSeq (PE-100) at Vanderbilt University Medical Center VANTAGE core. *Data Analysis:* Adaptors were trimmed with Trimmomatic-0.32 prior to aligning to the hg19 genome with Bowtie2 (v 2.2.2). Spike-in reads were removed and quantified. Bigwig files were generated using deepTools and normalized based on spike-in reads.

Supplementary Material

Refer to Web version on PubMed Central for supplementary material.

Acknowledgements

We thank the members of the Hiebert lab for helpful discussions, reagents and advice. We thank the VICC Flow Cytometry, Chemical Synthesis, and Genome Sciences Shared Resources for services and support. We also thank Mark Wunderlich and James Mulloy (Cincinnati Children's Hospital Medical Center) for helpful advice with the CD34+ cultures and Dr. H. Leighton Grimes (Cincinnati Children's Hospital Medical Center) for the Gfi1b plasmid. This work was supported by the T. J. Martell Foundation, the Robert J. Kleberg, Jr. and Helen C. Kleberg Foundation, National Institutes of Health grants (RO1-CA178030, RO1-CA164605 and R01-CA64140) and core services performed through Vanderbilt Digestive Disease Research grant (NIDDK P30DK58404) and the Vanderbilt-Ingram Cancer Center support grant (NCI P30CA68485), and the National Center for Advancing Translational Sciences, Grant 2 UL1 TR000445-06. Kristy Stengel was supported by 5 T32 CA009582-26 and a postdoctoral fellowship (PF-13-303-01-DMC) from the American Cancer Society.

Declaration of Interests

The authors declare no competing interests, although Scott Hiebert received research funding from Incyte Inc. through the Vanderbilt-Incyte Alliance. These funds did not support this work.

References

Amann JM, Nip J, Strom DK, Lutterbach B, Harada H, Lenny N, Downing JR, Meyers S, and Hiebert SW (2001). ETO, a target of t(8;21) in acute leukemia, makes distinct contacts with multiple histone deacetylases and binds mSin3A through its oligomerization domain. Mol Cell Biol 21, 6470–6483. [PubMed: 11533236]

Anguita E, Candel FJ, Chaparro A, and Roldan-Etcheverry JJ (2017). Transcription Factor GFI1B in Health and Disease. Front Oncol 7, 54. [PubMed: 28401061]

Ayatollahi H, Shajiei A, Sadeghian MH, Sheikhi M, Yazdandoust E, Ghazanfarpour M, Shams SF, and Shakeri S (2017). Prognostic Importance of C-KIT Mutations in Core Binding Factor Acute Myeloid Leukemia: A Systematic Review. Hematol Oncol Stem Cell Ther 10, 1–7. [PubMed: 27613372]

Berg T, Fliegauf M, Burger J, Staege MS, Liu S, Martinez N, Heidenreich O, Burdach S, Haferlach T, Werner MH, et al. (2008). Transcriptional upregulation of p21/WAF/Cip1 in myeloid leukemic blasts expressing AML1-ETO. Haematologica 93, 1728–1733. [PubMed: 18790797]

Bolger AM, Lohse M, and Usadel B (2014). Trimmomatic: a flexible trimmer for Illumina sequence data. Bioinformatics 30, 2114–2120. [PubMed: 24695404]

Chen M, Zhu N, Liu X, Laurent B, Tang Z, Eng R, Shi Y, Armstrong SA, and Roeder RG (2015). JMJD1C is required for the survival of acute myeloid leukemia by functioning as a coactivator for key transcription factors. Genes Dev 29, 2123–2139. [PubMed: 26494788]

Crans HN, and Sakamoto KM (2001). Transcription factors and translocations in lymphoid and myeloid leukemia. Leukemia 15, 313–331. [PubMed: 11237053]

Erickson P, Gao J, Chang KS, Look T, Whisenant E, Raimondi S, Lasher R, Trujillo J, Rowley J, and Drabkin H (1992). Identification of breakpoints in t(8;21) acute myelogenous leukemia and isolation of a fusion transcript, AML1/ETO, with similarity to Drosophila segmentation gene, runt. Blood 80, 1825–1831. [PubMed: 1391946]

Feng J, Liu T, Qin B, Zhang Y, and Liu XS (2012). Identifying ChIP-seq enrichment using MACS. Nat Protoc 7, 1728–1740. [PubMed: 22936215]

Gelmetti V, Zhang J, Fanelli M, Minucci S, Pelicci PG, and Lazar MA (1998). Aberrant recruitment of the nuclear receptor corepressor-histone deacetylase complex by the acute myeloid leukemia fusion partner ETO. Mol Cell Biol 18, 7185–7191. [PubMed: 9819405]

Heinz S, Benner C, Spann N, Bertolino E, Lin YC, Laslo P, Cheng JX, Murre C, Singh H, and Glass CK (2010). Simple combinations of lineage-determining transcription factors prime cis-regulatory elements required for macrophage and B cell identities. Mol Cell 38, 576–589. [PubMed: 20513432]

Henriques T, Scruggs BS, Inouye MO, Muse GW, Williams LH, Burkholder AB, Lavender CA, Fargo DC, and Adelman K (2018). Widespread transcriptional pausing and elongation control at enhancers. Genes Dev 32, 26–41. [PubMed: 29378787]

Hou HA, Chou WC, Kuo YY, Liu CY, Lin LI, Tseng MH, Chiang YC, Liu MC, Liu CW, Tang JL, et al. (2015). TP53 mutations in de novo acute myeloid leukemia patients: longitudinal follow-ups show the mutation is stable during disease evolution. Blood Cancer J 5, e331. [PubMed: 26230955]

Hsu PD, Lander ES, and Zhang F (2014). Development and applications of CRISPR-Cas9 for genome engineering. Cell 157, 1262–1278. [PubMed: 24906146]

Hunt A, Fischer M, Engel ME, and Hiebert SW (2011). Mtg16/Eto2 contributes to murine T-cell development. Molecular and cellular biology 31, 2544–2551. [PubMed: 21536648]

Jeanne M, Lallemand-Breitenbach V, Ferhi O, Koken M, Le Bras M, Duffort S, Peres L, Berthier C, Soilihi H, Raught B, et al. (2010). PML/RARA oxidation and arsenic binding initiate the antileukemia response of As2O3. Cancer Cell 18, 88–98. [PubMed: 20609355]

Jimenez JJ, Chale RS, Abad AC, and Schally AV (2020). Acute promyelocytic leukemia (APL): a review of the literature. Oncotarget 11, 992–1003. [PubMed: 32215187]

Johnston G, Ramsey HE, Liu Q, Wang J, Stengel KR, Sampathi S, Acharya P, Arrate M, Stubbs MC, Burn T, et al. (2020). Nascent transcript and single-cell RNA-seq analysis defines the mechanism of action of the LSD1 inhibitor INCB059872 in myeloid leukemia. Gene 752, 144758. [PubMed: 32422235]

Jongmans MC, Kuiper RP, Carmichael CL, Wilkins EJ, Dors N, Carmagnac A, Schouten-van Meeteren AY, Li X, Stankovic M, Kamping E, et al. (2010). Novel RUNX1 mutations in familial platelet disorder with enhanced risk for acute myeloid leukemia: clues for improved identification of the FPD/AML syndrome. Leukemia 24, 242–246. [PubMed: 19946261]

Jonkers I, Kwak H, and Lis JT (2014). Genome-wide dynamics of Pol II elongation and its interplay with promoter proximal pausing, chromatin, and exons. Elife 3, e02407. [PubMed: 24843027]

Jourdan E, Boissel N, Chevret S, Delabesse E, Renneville A, Cornillet P, Blanchet O, Cayuela JM, Recher C, Raffoux E, et al. (2013). Prospective evaluation of gene mutations and minimal residual disease in patients with core binding factor acute myeloid leukemia. Blood 121, 2213–2223. [PubMed: 23321257]

Kronke J, Udeshi ND, Narla A, Grauman P, Hurst SN, McConkey M, Svinkina T, Heckl D, Comer E, Li X, et al. (2014). Lenalidomide causes selective degradation of IKZF1 and IKZF3 in multiple myeloma cells. Science 343, 301–305. [PubMed: 24292625]

Lancrin C, Mazan M, Stefanska M, Patel R, Lichtinger M, Costa G, Vargel O, Wilson NK, Moroy T, Bonifer C, et al. (2012). GFI1 and GFI1B control the loss of endothelial identity of hemogenic endothelium during hematopoietic commitment. Blood 120, 314–322. [PubMed: 22668850]

Langmead B, and Salzberg SL (2012). Fast gapped-read alignment with Bowtie 2. Nat Methods 9, 357–359. [PubMed: 22388286]

Lee TI, and Young RA (2013). Transcriptional regulation and its misregulation in disease. Cell 152, 1237–1251. [PubMed: 23498934]

Li X, Xu YB, Wang Q, Lu Y, Zheng Y, Wang YC, Lubbert M, Zhao KW, and Chen GQ (2006). Leukemogenic AML1-ETO fusion protein upregulates expression of connexin 43: the role in AML 1-ETO-induced growth arrest in leukemic cells. J Cell Physiol 208, 594–601. [PubMed: 16741927]

Li Y, Wang H, Wang X, Jin W, Tan Y, Fang H, Chen S, Chen Z, and Wang K (2016). Genome-wide studies identify a novel interplay between AML1 and AML1/ETO in t(8;21) acute myeloid leukemia. Blood 127, 233–242. [PubMed: 26546158]

Liu Q, Wang J, Zhao Y, Li CI, Stengel KR, Acharya P, Johnston G, Hiebert SW, and Shyr Y (2017). Identification of active miRNA promoters from nuclear run-on RNA sequencing. Nucleic Acids Res 45, e121. [PubMed: 28460090]

Liu Y, Cheney MD, Gaudet JJ, Chruszcz M, Lukasik SM, Sugiyama D, Lary J, Cole J, Dauter Z, Minor W, et al. (2006). The tetramer structure of the Nervy homology two domain, NHR2, is critical for AML1/ETO's activity. Cancer Cell 9, 249–260. [PubMed: 16616331]

Loke J, Assi SA, Imperato MR, Ptasinska A, Cauchy P, Grabovska Y, Soria NM, Raghavan M, Delwel HR, Cockerill PN, et al. (2017). RUNX1-ETO and RUNX1-EVI1 Differentially Reprogram the Chromatin Landscape in t(8;21) and t(3;21) AML. Cell Rep 19, 1654–1668. [PubMed: 28538183]

Love MI, Huber W, and Anders S (2014). Moderated estimation of fold change and dispersion for RNA-seq data with DESeq2. Genome Biol 15, 550. [PubMed: 25516281]

Lu G, Middleton RE, Sun H, Naniong M, Ott CJ, Mitsiades CS, Wong KK, Bradner JE, and Kaelin WG Jr. (2014). The myeloma drug lenalidomide promotes the cereblon-dependent destruction of Ikaros proteins. Science 343, 305–309. [PubMed: 24292623]

Lutterbach B, Sun D, Schuetz J, and Hiebert SW (1998a). The MYND motif is required for repression of basal transcription from the multidrug resistance-1 promoter by the t(8;21) fusion protein. Mol. Cell. Biol. 18, 3601–3611.

Lutterbach B, Westendorf JJ, Linggi B, Patten A, Moniwa M, Davie JR, Huynh KD, Bardwell VJ, Lavinsky RM, Rosenfeld MG, et al. (1998b). ETO, a target of t(8;21) in acute leukemia, interacts with the N-CoR and mSin3 corepressors. Mol Cell Biol 18, 7176–7184. [PubMed: 9819404]

Mahat DB, Kwak H, Booth GT, Jonkers IH, Danko CG, Patel RK, Waters CT, Munson K, Core LJ, and Lis JT (2016). Base-pair-resolution genome-wide mapping of active RNA polymerases using precision nuclear run-on (PRO-seq). Nat Protoc 11, 1455–1476. [PubMed: 27442863]

Maiques-Diaz A, Spencer GJ, Lynch JT, Ciceri F, Williams EL, Amaral FMR, Wiseman DH, Harris WJ, Li Y, Sahoo S, et al. (2018). Enhancer Activation by Pharmacologic Displacement of LSD1 from GFI1 Induces Differentiation in Acute Myeloid Leukemia. Cell Rep 22, 3641–3659. [PubMed: 29590629]

Martens JH, Mandoli A, Simmer F, Wierenga BJ, Saeed S, Singh AA, Altucci L, Vellenga E, and Stunnenberg HG (2012). ERG and FLI1 binding sites demarcate targets for aberrant epigenetic regulation by AML1-ETO in acute myeloid leukemia. Blood 120, 4038–4048. [PubMed: 22983443]

Martinez-Soria N, McKenzie L, Draper J, Ptasinska A, Issa H, Potluri S, Blair HJ, Pickin A, Isa A, Chin PS, et al. (2018a). The Oncogenic Transcription Factor RUNX1/ETO Corrupts Cell Cycle Regulation to Drive Leukemic Transformation. Cancer Cell 34, 626–642 e628. [PubMed: 30300583]

Martinez-Soria N, McKenzie L, Draper J, Ptasinska A, Issa H, Potluri S, Blair HJ, Pickin A, Isa A, Chin PS, et al. (2018b). The Oncogenic Transcription Factor RUNX1/ETO Corrupts Cell Cycle Regulation to Drive Leukemic Transformation. Cancer Cell 34, 626–642 e628. [PubMed: 30300583]

Melnikova IN, Crute BE, Wang S, and Speck NA (1993). Sequence specificity of the core-binding factor. J Virol 67, 2408–2411. [PubMed: 8445737]

Meyers S, Downing JR, and Hiebert SW (1993). Identification of AML-1 and the (8;21) translocation protein (AML-1/ETO) as sequence-specific DNA-binding proteins: the runt homology domain is required for DNA binding and protein-protein interactions. Mol Cell Biol 13, 6336–6345. [PubMed: 8413232]

Miyoshi H, Kozu T, Shimizu K, Enomoto K, Maseki N, Kaneko Y, Kamada N, and Ohki M (1993). The t(8;21) translocation in acute myeloid leukemia results in production of an AML1-MTG8 fusion transcript. EMBO J 12, 2715–2721. [PubMed: 8334990]

Miyoshi H, Shimizu K, Kozu T, Maseki N, Kaneko Y, and Ohki M (1991). t(8;21) breakpoints on chromosome 21 in acute myeloid leukemia are clustered within a limited region of a single gene, AML1. Proc Natl Acad Sci U S A 88, 10431–10434. [PubMed: 1720541]

Muhar M, Ebert A, Neumann T, Umkehrer C, Jude J, Wieshofer C, Rescheneder P, Lipp JJ, Herzog VA, Reichholf B, et al. (2018). SLAM-seq defines direct gene-regulatory functions of the BRD4-MYC axis. Science 360, 800–805. [PubMed: 29622725]

Mulloy JC, Cammenga J, Berguido FJ, Wu K, Zhou P, Comenzo RL, Jhanwar S, Moore MA, and Nimer SD (2003). Maintaining the self-renewal and differentiation potential of human CD34+ hematopoietic cells using a single genetic element. Blood 102, 4369–4376. [PubMed: 12946995]

Nabet B, Roberts JM, Buckley DL, Paulk J, Dastjerdi S, Yang A, Leggett AL, Erb MA, Lawlor MA, Souza A, et al. (2018). The dTAG system for immediate and target-specific protein degradation. Nat Chem Biol 14, 431–441. [PubMed: 29581585]

Nafria M, Keane P, Ng ES, Stanley EG, Elefanty AG, and Bonifer C (2020). Expression of RUNX1-ETO Rapidly Alters the Chromatin Landscape and Growth of Early Human Myeloid Precursor Cells. Cell Rep 31, 107691. [PubMed: 32460028]

Nasr R, Guillemin MC, Ferhi O, Soilihi H, Peres L, Berthier C, Rousselot P, Robledo-Sarmiento M, Lallemand-Breitenbach V, Gourmel B, et al. (2008). Eradication of acute promyelocytic leukemia-initiating cells through PML-RARA degradation. Nat Med 14, 1333–1342. [PubMed: 19029980]

Ogawa E, Maruyama M, Kagoshima H, Inuzuka M, Lu J, Satake M, Shigesada K, and Ito Y (1993). PEBP2/PEA2 represents a family of transcription factors homologous to the products of the Drosophila runt gene and the human AML1 gene. Proc Natl Acad Sci U S A 90, 6859–6863. [PubMed: 8341710]

Perry JA, Seong BKA, and Stegmaier K (2019). Biology and Therapy of Dominant Fusion Oncoproteins Involving Transcription Factor and Chromatin Regulators in Sarcomas. Annu Rev Canc Biol 3, 299–321.

Peterson LF, and Zhang DE (2004). The 8;21 translocation in leukemogenesis. Oncogene 23, 4255–4262. [PubMed: 15156181]

Plevin MJ, Zhang J, Guo C, Roeder RG, and Ikura M (2006). The acute myeloid leukemia fusion protein AML1-ETO targets E proteins via a paired amphipathic helix-like TBP-associated factor homology domain. Proc Natl Acad Sci U S A 103, 10242–10247. [PubMed: 16803958]

Ptasinska A, Assi SA, Mannari D, James SR, Williamson D, Dunne J, Hoogenkamp M, Wu M, Care M, McNeill H, et al. (2012). Depletion of RUNX1/ETO in t(8;21) AML cells leads to genome-wide changes in chromatin structure and transcription factor binding. Leukemia 26, 1829–1841. [PubMed: 22343733]

Ptasinska A, Assi SA, Martinez-Soria N, Imperato MR, Piper J, Cauchy P, Pickin A, James SR, Hoogenkamp M, Williamson D, et al. (2014). Identification of a dynamic core transcriptional network in t(8;21) AML that regulates differentiation block and self-renewal. Cell Rep 8, 1974–1988. [PubMed: 25242324]

Ptasinska A, Pickin A, Assi SA, Chin PS, Ames L, Avellino R, Groschel S, Delwel R, Cockerill PN, Osborne CS, et al. (2019). RUNX1-ETO Depletion in t(8;21) AML Leads to C/EBPalpha- and AP-1-Mediated Alterations in Enhancer-Promoter Interaction. Cell Rep 29, 2120. [PubMed: 31722222]

Ramirez F, Ryan DP, Gruning B, Bhardwaj V, Kilpert F, Richter AS, Heyne S, Dundar F, and Manke T (2016). deepTools2: a next generation web server for deep-sequencing data analysis. Nucleic Acids Res 44, W160–165. [PubMed: 27079975]

Ross-Innes CS, Stark R, Teschendorff AE, Holmes KA, Ali HR, Dunning MJ, Brown GD, Gojis O, Ellis IO, Green AR, et al. (2012). Differential oestrogen receptor binding is associated with clinical outcome in breast cancer. Nature 481, 389–393. [PubMed: 22217937]

Roth S, Fulcher LJ, and Sapkota GP (2019). Advances in targeted degradation of endogenous proteins. Cell Mol Life Sci 76, 2761–2777. [PubMed: 31030225]

Sampathi S, Acharya P, Zhao Y, Wang J, Stengel KR, Liu Q, Savona MR, and Hiebert SW (2019). The CDK7 inhibitor THZ1 alters RNA polymerase dynamics at the 5' and 3' ends of genes. Nucleic Acids Res 47, 3921–3936. [PubMed: 30805632]

Schenk T, Chen WC, Gollner S, Howell L, Jin L, Hebestreit K, Klein HU, Popescu AC, Burnett A, Mills K, et al. (2012). Inhibition of the LSD1 (KDM1A) demethylase reactivates the all-trans-retinoic acid differentiation pathway in acute myeloid leukemia. Nat Med 18, 605–611. [PubMed: 22406747]

Schoenherr C, Wohlan K, Dallmann I, Pich A, Hegermann J, Ganser A, Hilfiker-Kleiner D, Heidenreich O, Scherr M, and Eder M (2019). Stable depletion of RUNX1-ETO in Kasumi-1 cells induces expression and enhanced proteolytic activity of Cathepsin G and Neutrophil Elastase. PLoS One 14, e0225977. [PubMed: 31826021]

Skene PJ, Henikoff JG, and Henikoff S (2018). Targeted in situ genome-wide profiling with high efficiency for low cell numbers. Nat Protoc 13, 1006–1019. [PubMed: 29651053]

Spirin PV, Lebedev TD, Orlova NN, Gornostaeva AS, Prokofjeva MM, Nikitenko NA, Dmitriev SE, Buzdin AA, Borisov NM, Aliper AM, et al. (2014). Silencing AML1-ETO gene expression leads to simultaneous activation of both pro-apoptotic and proliferation signaling. Leukemia 28, 2222–2228. [PubMed: 24727677]

Sun XJ, Wang Z, Wang L, Jiang Y, Kost N, Soong TD, Chen WY, Tang Z, Nakadai T, Elemento O, et al. (2013). A stable transcription factor complex nucleated by oligomeric AML1-ETO controls leukaemogenesis. Nature 500, 93–97. [PubMed: 23812588]

Trapnell C, Hendrickson DG, Sauvageau M, Goff L, Rinn JL, and Pachter L (2013). Differential analysis of gene regulation at transcript resolution with RNA-seq. Nat Biotechnol 31, 46–53. [PubMed: 23222703]

Trombly DJ, Whitfield TW, Padmanabhan S, Gordon JA, Lian JB, van Wijnen AJ, Zaidi SK, Stein JL, and Stein GS (2015). Genome-wide co-occupancy of AML1-ETO and N-CoR defines the t(8;21) AML signature in leukemic cells. BMC Genomics 16, 309. [PubMed: 25928846]

van Bergen M, and van der Reijden BA (2019). Targeting the GFI1/1B-CoREST Complex in Acute Myeloid Leukemia. Front Oncol 9, 1027. [PubMed: 31649884]

Vangala RK, Heiss-Neumann MS, Rangatia JS, Singh SM, Schoch C, Tenen DG, Hiddemann W, and Behre G (2003). The myeloid master regulator transcription factor PU.1 is inactivated by AML1-ETO in t(8;21) myeloid leukemia. Blood 101, 270–277. [PubMed: 12393465]

Wang J, Hoshino T, Redner RL, Kajigaya S, and Liu JM (1998). ETO, fusion partner in t(8;21) acute myeloid leukemia, represses transcription by interaction with the human N-CoR/mSin3/HDAC1 complex. Proc Natl Acad Sci U S A 95, 10860–10865. [PubMed: 9724795]

Wang J, Zhao Y, Zhou X, Hiebert SW, Liu Q, and Shyr Y (2018). Nascent RNA sequencing analysis provides insights into enhancer-mediated gene regulation. BMC Genomics 19, 633. [PubMed: 30139328]

Wang L, Gural A, Sun XJ, Zhao X, Perna F, Huang G, Hatlen MA, Vu L, Liu F, Xu H, et al. (2011). The leukemogenicity of AML1-ETO is dependent on site-specific lysine acetylation. Science 333, 765–769. [PubMed: 21764752]

Warrell RP Jr., Frankel SR, Miller WH Jr., Scheinberg DA, Itri LM, Hittelman WN, Vyas R, Andreeff M, Tafuri A, Jakubowski A, et al. (1991). Differentiation therapy of acute promyelocytic leukemia with tretinoin (all-trans-retinoic acid). N Engl J Med 324, 1385–1393. [PubMed: 1850498]

Weintraub AS, Li CH, Zamudio AV, Sigova AA, Hannett NM, Day DS, Abraham BJ, Cohen MA, Nabet B, Buckley DL, et al. (2017). YY1 Is a Structural Regulator of Enhancer-Promoter Loops. Cell 171, 1573–1588 e1528. [PubMed: 29224777]

Wissink EM, Vihervaara A, Tippens ND, and Lis JT (2019). Nascent RNA analyses: tracking transcription and its regulation. Nat Rev Genet 20, 705–723. [PubMed: 31399713]

Wunderlich M, and Mulloy JC (2009). Model systems for examining effects of leukemia-associated oncogenes in primary human CD34+ cells via retroviral transduction. Methods Mol Biol 538, 263–285. [PubMed: 19277588]

Yan M, Kanbe E, Peterson LF, Boyapati A, Miao Y, Wang Y, Chen IM, Chen Z, Rowley JD, Willman CL, et al. (2006). A previously unidentified alternatively spliced isoform of t(8;21) transcript promotes leukemogenesis. Nat Med 12, 945–949. [PubMed: 16892037]

Zhang J, Kalkum M, Yamamura S, Chait BT, and Roeder RG (2004). E protein silencing by the leukemogenic AML1-ETO fusion protein. Science 305, 1286–1289. [PubMed: 15333839]

Zhao Y, Liu Q, Acharya P, Stengel KR, Sheng Q, Zhou X, Kwak H, Fischer MA, Bradner JE, Strickland SA, et al. (2016). High-Resolution Mapping of RNA Polymerases Identifies Mechanisms of Sensitivity and Resistance to BET Inhibitors in t(8;21) AML. Cell Rep 16, 2003–2016. [PubMed: 27498870]

Highlights

- A chemical genetic approach allows rapid degradation of endogenous AML1-ETO
- Nascent transcript analysis identifies ~60 direct targets of AML1-ETO repression
- AML1-ETO only antagonizes RUNX1 binding to suppress H3K27ac at select sites
- Reactivation of *GFI1B* cooperates with AML1-ETO loss to promote differentiation

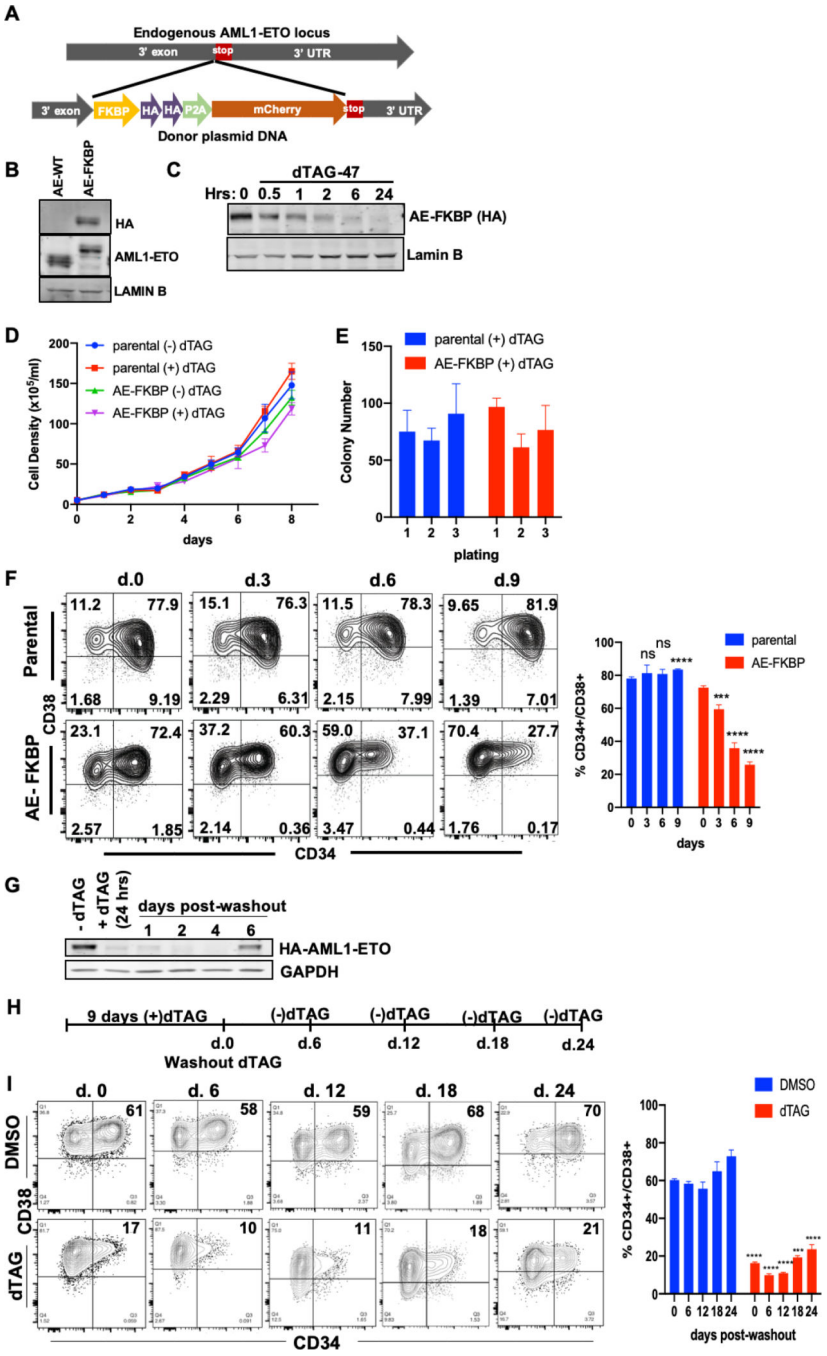

Figure 1. Targeting of an FKBP12-F36V degron tag to the endogenous AML1-ETO locus allows protein degradation upon dTAG-47 treatment.

(A) Schematic depicting CRISPR-HDR based targeting approach. (B) Western blot from lysates of parental (AE-WT) or AML1-ETO-FKBP12^{F36V}-2xHA (AE-FKBP) Kasumi-1 cells. α-HA (detects AE-FKBP) and α-Runt homology domain (detects AE-WT and AE-FKBP). (C) Kasumi-1-AE-FKBP cells were treated with 500 nM dTAG-47 for the indicated times and protein levels monitored by blotting with α-HA. (D) Cells were treated with 500 nM dTAG-47 for 8 days and growth monitored by cell counts. (E) Cells were cultured in the presence of 500 nM dTAG-47 for 24hr and plated in methylcellulose in the presence of 500

nM dTAG-47. Colonies were counted and replated every 12 days. (F). Cells were analyzed for surface CD34 and CD38 expression by flow cytometry over 9 days of dTAG-47 treatment. Quantification depicted at right. (G) Western blot analysis of AML1-ETO-FKBP after treatment or "washout" of dTAG-47 for 1–6 days. (H) Schematic diagram of the experimental design of the long-term "washout" experiment. (I) FACS analysis to measure the state of differentiation of Kasumi-1 cells at the times indicated in (H). The numbers in the upper right quadrant indicate the percentage of cells and quantification is depicted at right. ***$p \leq 0.001$, ****$p \leq 0.0001$.

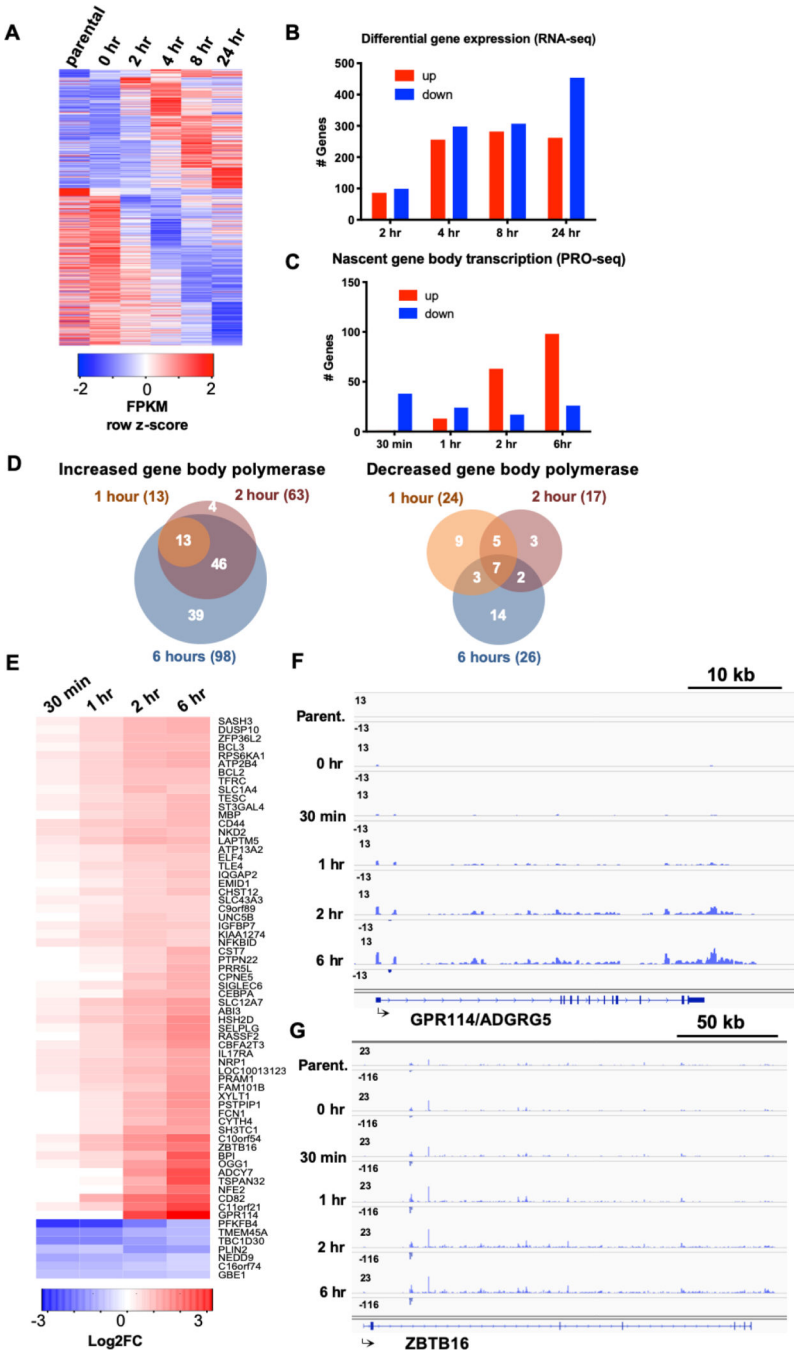

Figure 2. AML1-ETO represses the expression of fewer than one-hundred genes.

(A) RNA-seq was performed at the indicated timepoints following dTAG-47 treatment. Heatmap depicts genes changed in at least one timepoint. (B) Quantitation of the number of genes identified as significantly up-regulated (up > 1.5-fold; q<0.05) or down-regulated (down > 1.5-fold; q<0.05) by RNA-seq. (C) Quantitation of the number of genes with increases (up > 1.5-fold; q<0.05) or decreases (down > 1.5-fold; q<0.05) in gene transcription as identified by PRO-seq. (D) Venn diagrams depict the overlap of genes exhibiting increased or decreased transcription by PRO-seq at 1, 2, and 6hr following

AML1-ETO degradation. (E) Heatmap showing the change in gene transcription of 59 up-regulated genes and 7 down-regulated genes identified by PRO-seq over time compared with 0hr. controls. Screenshots illustrate changes in PRO-seq signal at the *GPR114/ADGRG5* (F) and *ZBTB16* (G) loci over time.

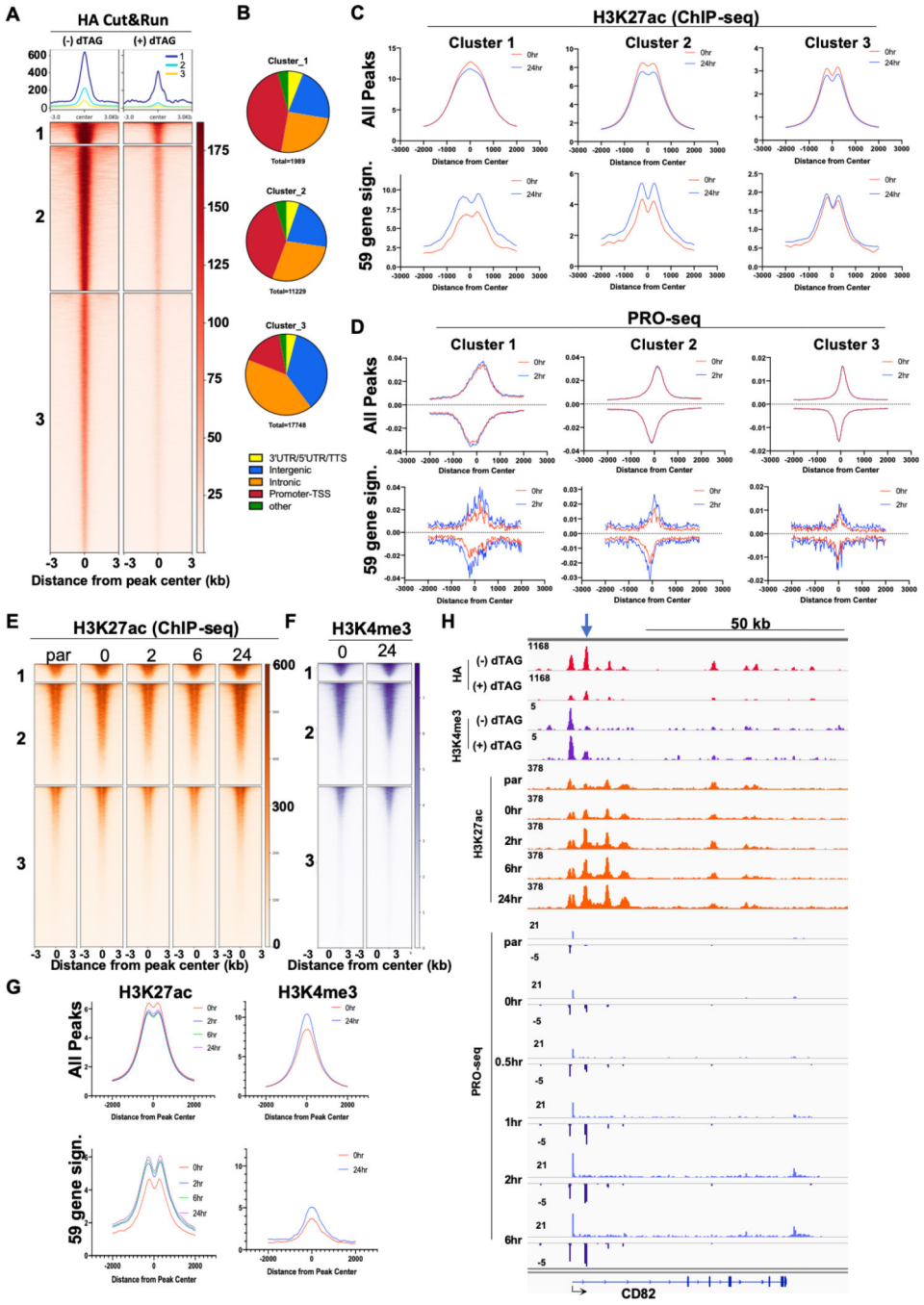

Figure 3. Intersection of AML1-ETO binding with PRO-seq and histone marks define high-confidence AML1-ETO targets.

(A) CUT&RUN analysis was performed using α-HA to detect AML1-ETO-FKBP12^{F36V}-2xHA binding before and after 18hr treatment with 500 nM dTAG-47. Peaks identified as significantly changed after dTAG-treatment by DiffBind are depicted in the heatmap. K-means clustering was used to segment peaks based on signal intensity (Clusters 1–3). (B) and the relative location of binding sites for each cluster identified. (C) Histograms depict the change in H3K27ac signal around HA-peaks following a 24hr dTAG treatment. The H3K27ac ChIP-seq signal was plotted for +/− 2kb around all HA-peak centers for each

cluster (upper) or plotted only for peaks associated with the 59-gene AML1-ETO repression signature identified in Figure 2 (lower). (D) PRO-seq signal at 0hr and 2hr following dTAG treatment plotted as in (C). Heatmaps of H3K27ac (E) and H3K4me3 (F) around HA-AML1-ETO peaks identified in A. (G) Histograms depict the change in H3K27ac and H3K4me3 around all AML1-ETO-FKPB-HA peaks or the 59 genes activated following dTAG-47 treatment. (H) Screenshot of the *CD82* locus. Blue arrow indicates the intergenic enhancer.

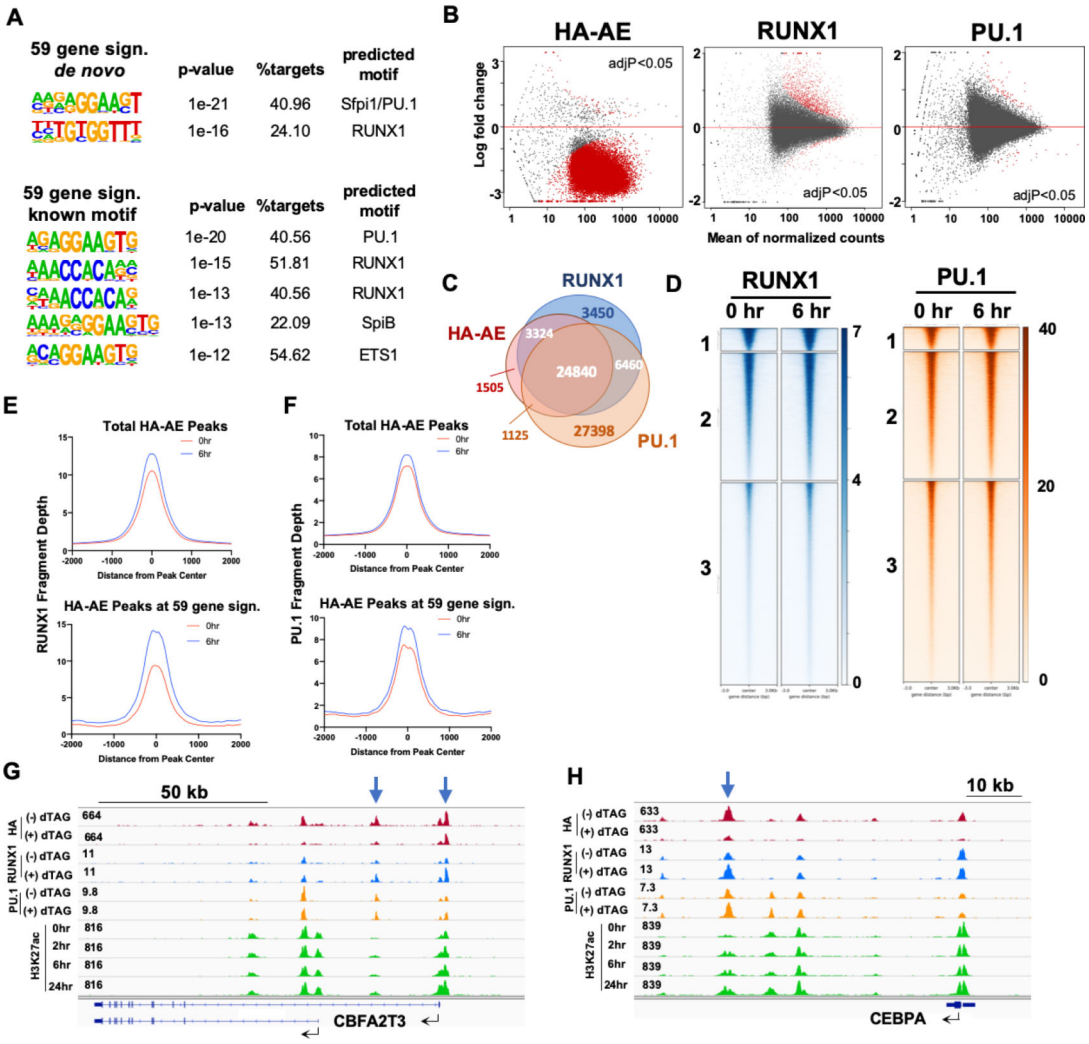

Figure 4. RUNX1 rapidly and selectively replaces AML1-ETO upon degradation.

(A) *De novo* and known motif analysis (HOMER) of the AML1-ETO peaks associated with the 59 genes activated after degradation of the fusion protein. (B) Scatter plots of the AML1-ETO-FKBP-HA, RUNX1 and the PU.1 CUT&RUN peaks showing the Log2 fold change after degradation of the fusion protein by dTAG-47. Red indicates peaks that reached statistical significance. (C) Venn diagram showing the overlapping or non-overlapping peaks for AML1-ETO (HA-AE), RUNX1 and PU.1. (D) Heat maps depicting the RUNX1 and PU.1 CUT&RUN signal around the HA-AML1-ETO peaks depicted in Figure 3A. (E and F) Histograms showing the fragment depth of RUNX1 (E) or PU.1 (F) peaks at all AML1-ETO-HA peaks (upper panels) or the AML1-ETO peaks associated with the 59 genes activated upon AML1-ETO degradation. IGV screenshots showing the CBFA2T3 (ETO2 or MTG16) locus (G) and the CEBPA locus (H). The blue arrows identify peaks bound by AML1-ETO and with increased RUNX1 occupancy following AML1-ETO degradation.

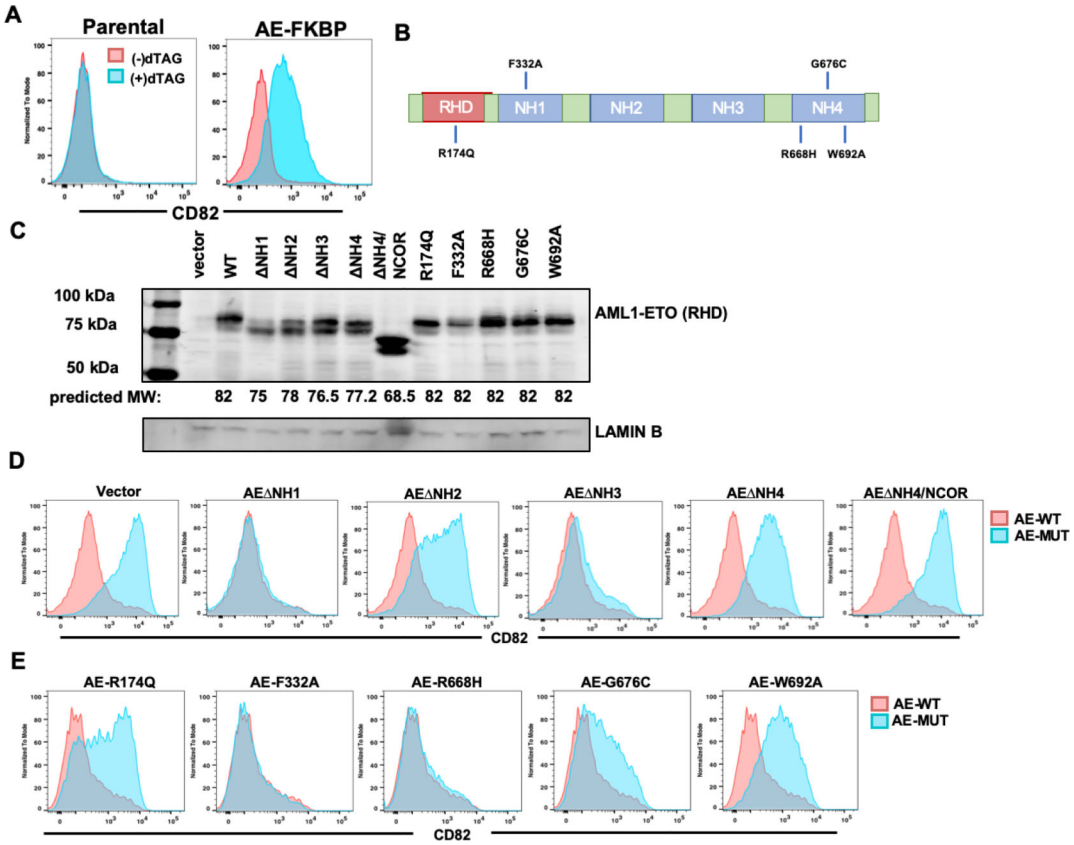

Figure 5. CD82 serves as a reporter for AML1-ETO-mediated repression.

(A) Flow cytometry for surface CD82 protein following 24hr dTAG-47 treatment. (B) Diagram illustrates AML1-ETO domain structure and the location of point mutations generated. (C) Western blot shows the expression of wild-type (WT) AML1-ETO and the indicated point mutants or domain deletion mutants. Predicted molecular weights are listed under each lane. CD82 protein levels were determined by flow cytometry to determine the ability of domain deletion mutations (D) or point mutations (E) to complement AML1-ETO degradation relative to WT-AML1-ETO.

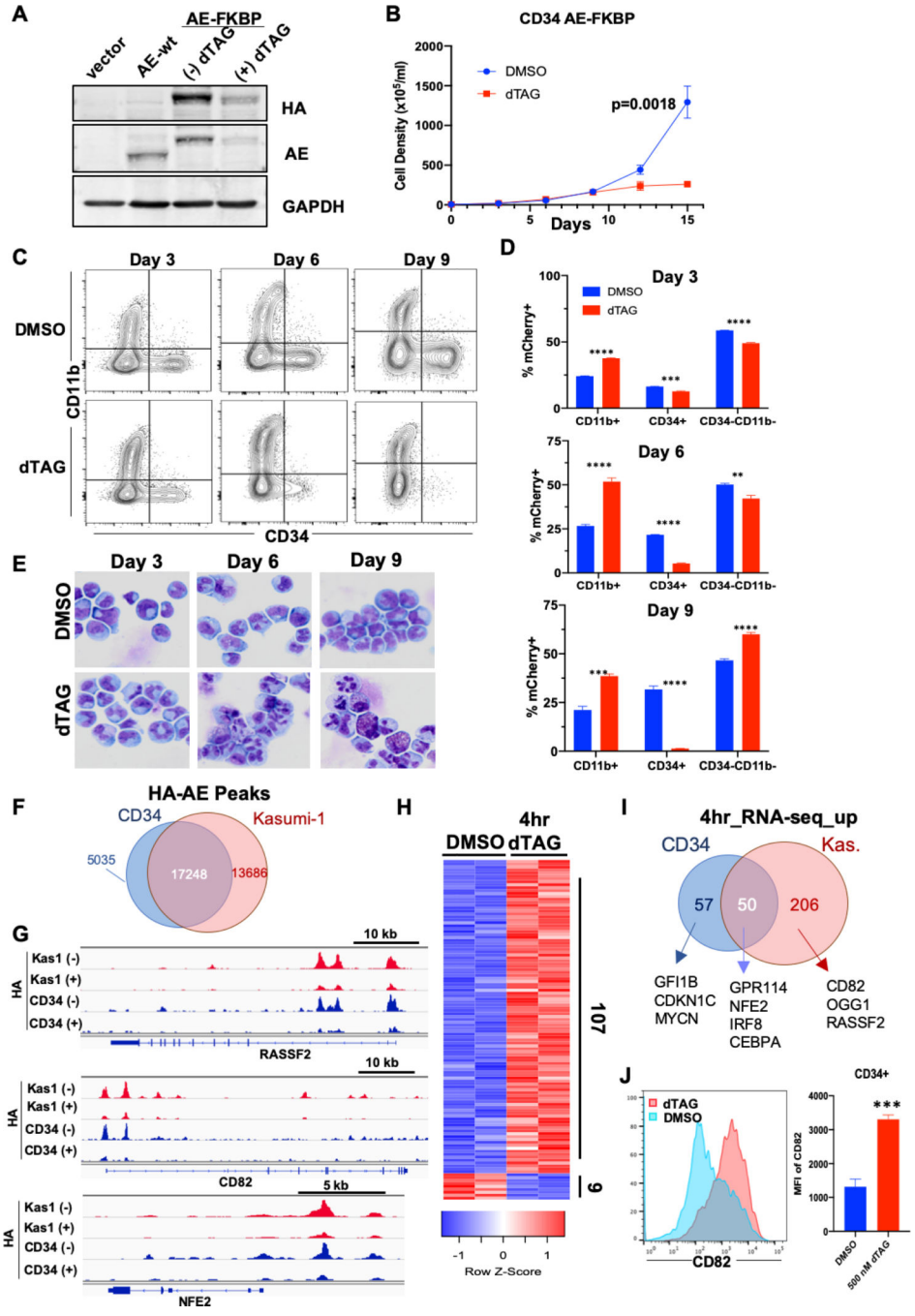

Figure 6. Maintained AML1-ETO-expression is required to suppress differentiation of CD34^{+} HSPCs.

(A) CD34^{+} human cord blood cells expressing AML1-ETO, AML1-ETO-FKBP12^{F36V}-2xHA (AE-FKBP), or vector control were treated with 500 nM dTAG-47 overnight and western blot used to assess AML1-ETO protein degradation. (B) Growth curves were performed in the presence of dTAG-47 or DMSO control. (C) Flow cytometry was performed on 3, 6 and 9-days post-treatment with dTAG-47 to monitor CD34 and CD11b expression. The results are quantified in (D). (E) Cytospins and Wright-Giemsa staining were performed every three days on AML1-ETO-FKBP cultures. (F) CUT&RUN

analysis utilizing α-HA to detect AML1-ETO-FKBP binding sites in $CD34^+$ HSPC cultures. A Venn diagram illustrates the overlap of peaks in Kasumi-1 cells and $CD34^+$ HSPC cultures. (G) Screenshots show examples of common AML1-ETO-binding sites in Kasumi-1 cells and CD34 cultures at the *RASSF2*, *CD82*, and *NFE2* loci. (H) RNA-seq was performed at 4hr post-treatment. The heatmap shows genes significantly changed by greater than 1.5-fold. The 107 genes significantly up-regulated upon AML1-ETO-FKBP degradation (up > 1.5-fold; $q<0.05$) were compared with the genes identified by RNA-seq as up-regulated by 4hr in Kasumi-1 cells (I). (J) Flow cytometry for CD82 shows a significant increase in CD82 protein levels 24hr following dTAG treatment. ***$p\leq0.001$, ****$p\leq0.0001$.

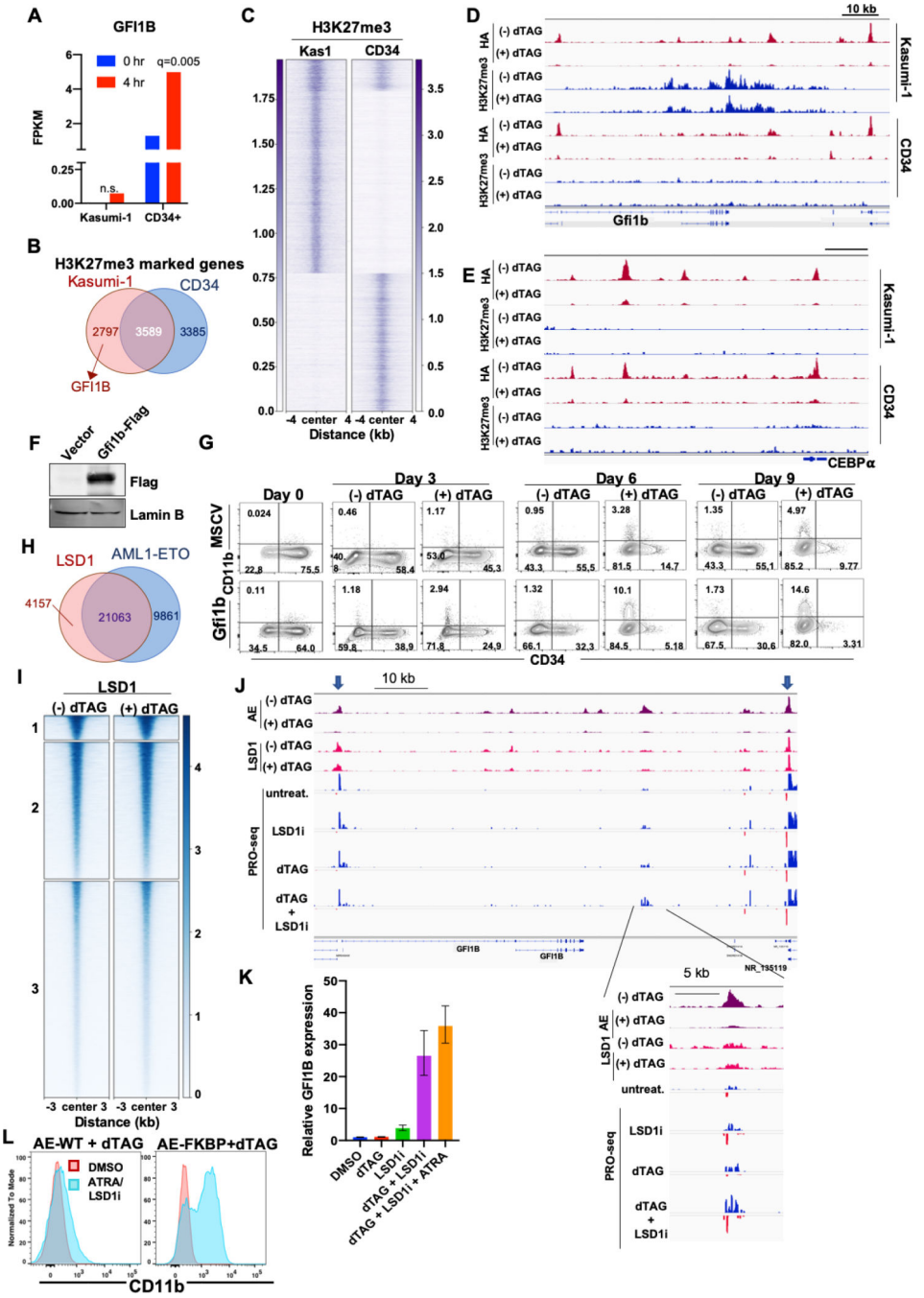

Figure 7. GFI1B is marked by H3K27me3 in Kasumi-1, but not CD34+ cells expressing AML1-ETO.

(A) RNA-seq revealed a significant increase in *GFI1B* expression following AML1-ETO degradation in CD34 cells, but not Kasumi-1 cells. (B and C) CUT&RUN analysis of H3K27me3 in Kasumi-1 and CD34+ HSPCs expressing AML1-ETO-FKBP-HA. (B) Venn diagram shows H3K27me3 marked genes that overlap between these cell types. (C) Heat maps of CUT&RUN peaks in Kasumi-1 (left) or CD34+ AML1-ETO expressing cells (right). (D and E) IGV screenshots of an AML1-ETO target gene unique to $CD34^{+}$ cells (*GFI1B;* D) and an AML1-ETO target gene shared between Kasumi-1 and $CD34^{+}$ cells

(*CEBPA;* E) (F) Western blot analysis showing Gfi1b expressed from MSCV in Kasumi-1 cells. (G) FACS analysis of Kasumi-1 cells infected with MSCV-GFP or MSCV-Gfi1b-GFP at 3, 6, and 9 days following dTAG treatment (H and I) CUT&RUN analysis of LSD1 from Kasumi-1 cells. (H) Venn diagram showing overlap of LSD1 and AML1-ETO peaks. (I) LSD1 signal around HA-AML1-ETO peaks depicted in Fig. 3A before and after degradation of AML1-ETO-FKBP. (J) IGV screenshot of GFI1B showing the location of AML1-ETO and LSD1 peaks relative to active RNA polymerase measured by PROseq before and after treatment of with LSD1 inhibitor, dTAG-47 or the combination thereof. (K) Q-RT-PCR was performed to determine the relative expression of *GFI1B* compared to *Actb* control. Expression is shown relative to DMSO treated cells and error bars represent the RQ_{min} and RQ_{max}. (L) Flow cytometry detecting CD11B expression in parental Kasumi-1 cells or AML1-ETO-FKBP Kasumi-1 cells that were treated with dTAG-47 alone or in combination with 100 nM GSK2879552 and 1 μM ATRA.

KEY RESOURCES TABLE

REAGENT or RESOURCE	SOURCE	IDENTIFIER
Antibodies		
α-HA tag [HA.C5]	Abcam	CAT# ab18181; RRID: AB_444303
αLamin B (M-20)	Santa Cruz	CAT# sc-6217; RRID: AB_648158
α-IKAROS Antibody (E2)	Santa Cruz	CAT# sc-398265
α-GAPDH Antibody (G9)	Santa Cruz	CAT# sc-365062; RRID: AB_10847862
α-Runt Homology Domain (RHD)	Made in house	N/A
α-CD82 Alexa Fluor 647	Fisher Scientific	CAT# BDB561341; RRID: AB_2738755
α-CD11b/MAC-1 Clone ICRF44 APC	Fisher Scientific	CAT# BDB550019; RRID: AB_398456
α-CD34 FITC Clone 581	Fisher Scientific	CAT# BDB555821; RRID: AB_396150
α-CD34 BV421 Clone 581	Fisher Scientific	CAT# BD562577; RRID: AB_2687922
α-CD38 APC CloneHIT2	Fisher Scientific	CAT# BDB555462; RRID: AB_398599
α-HA-Tag (C29F4) Rabbit mAB	Cell Signaling Technology	CAT# 3724S; RRID: AB_1549585
Donkey α-Rabbit IgG (H+L) Cross-Adsorbed Secondary Antibody	Invitrogen	CAT# 31238; RRID: AB_429690
α-ETO	Made in house	N/A
α-Histone H3 (acetyl K27) antibody-ChIP Grade	Abcam	CAT# ab4729; RRID: AB_2118291
α-H3K4me3	Abcam	CAT# ab12209; RRID: AB_442957
α-H3K27me3	Cell Signaling Technology	CAT# 9733l RRID: AB_2616029
α-RUNX1	Santa Cruz	CAT# sc-365644; RRID: AB_10843207
α-PU.1	Santa Cruz	CAT# sc-390405
α-LSD1	Abcam	CAT# ab 17721; RRID: AB_443964
Rabbit α-Mouse IgG	Abcam	CAT# ab46540
Bacterial and Virus Strains		
Biological Samples		
Chemicals, Peptides, and Recombinant Proteins		
RPMI	Fisher Scientific	CAT#MT15040CV
FetalPlex	Gemini Bio-Products	CAT#100–602
Corning Penicillin/Streptomycin	Fisher Scientific	CAT#MT30002CI
Corning L-glutamine Solution	Fisher Scientific	CAT#MT25005CI
IMDM	Fisher Scientific	CAT#12440053
Fetal Bovine Serum	R&D Systems	CAT#S11150
2-Mercaptoethanol	Fisher Scientific	CAT#21985023; CAS: 60–24-2
SCF	PeproTech	CAT#300–07

REAGENT or RESOURCE	SOURCE	IDENTIFIER
TPO	PeproTech	CAT#300–18
Flt3-L	PeproTech	CAT#300–19
IL-3	PeproTech	CAT#200–03
IL-6	PeproTech	CAT#200–06
dTAG-47	Vanderbilt Chemical Synthesis Core	Custom dTAG-47 Synthesis
DMSO	MilliporeSigma	CAT#D8418; CAS: 67–68-5
PEI	Polysciences	CAT#23966; CAS: 9002–98-6, 26913–06-4
Polybrene	MilliporeSigma	CAT#H9268; CAS: 28728–55-4
LSD1 inhibitor (GSK2879552)	SelleckChem	CAT#S7796; CAS: 1902123–72-1
ATRA	MilliporeSigma	CAT#R2625; CAS: 302–79-4
Trizol	ThermoFisher	CAT#15596026; CAS: 108–95-2, 1762–95-4, 593–84-0
SYBR Green	BioRad	CAT#1708880
MethoCult H4434 Classic	StemCell Technologies	CAT#04434
Phenol:Chloroform:Isoamyl Alcohol	MilliporeSigma	CAT#P3803; CAS: 108–95-2, 67–66-3, 123–51-3
Biotin-11-CTP	PerkinElmer	CAT#NEL542001EA
Digitonin	MilliporeSigma	CAT#300410, CAS: 11024–24-1
BioMag Plus Concanavalin A Beads	Bangs Laboratories, Inc	CAT#BP531
Dynabeads Protein A	ThermoFisher	CAT#10001D
Dynabeads Protein G	ThermoFisher	CAT#10003D
Sodium hydroxide	Fisher Scientific	CAT#BP359; CAS: 1310–73-2
Sarkosyl	Fisher Scientific	CAT#IB07080; CAS: 7631–98-3
Glycine	Fisher Scientific	CAT#808831; CAS: 56–40-6
Formaldehyde	MilliporeSigma	CAT#F1635; CAS: 50–00-0
Critical Commercial Assays		
QuickChange Lightning Site-Directed Mutagenesis kit	Agilent	CAT#210518
High Capacity cDNA Reverse Transcription Kit	ThermoFisher	CAT#4368814
NEBNext Ultra II DNA Library Prep Kit	NEB	CAT#E7645
Hema 3 Stat Pack	Fisher Healthcare	CAT# 123–869
Gibson Assembly Cloning kit	NEB	CAT# E5510S
Qiagen QIAfilter Maxi Kit	Qiagen	CAT# 12263
Deposited Data		
Raw and analyzed data	This paper	GEO: GSE153281
Raw Data	This paper; Mendeley Data	https://data.mendeley.com/datasets/3z2g7cs2ht/draft?a=05c22fa8-bd6b-4f3b-9788-c16dc6adfe83
Experimental Models: Cell Lines		

REAGENT or RESOURCE	SOURCE	IDENTIFIER
Kasumi-1	ATCC	CAT#CRL-2724; RRID: CVCL_0589
Human Cord Blood CD34+ Cells, Mixed (1x10e6)	StemCell Technologies	CAT#70008
Kasumi-1-AML1-ETO-FKBP12^{F36V}	This paper	N/A
293T	ATCC	CAT#CRL-3216; RRID: CVCL_0063
Experimental Models: Organisms/Strains		
Oligonucleotides		
Alt-R® CRISPR-Cas9 tracrRNA	Integrated DNA Technologies	CAT#1072534
crRNA Runx1t1 (ETO): TCTGAGTTCACGTCTAGCGA	Integrated DNA Technologies	CAT#Alt-R® CRISPR-Cas9 crRNA
Integrated DNA Technologies	Integrated DNA Technologies	Custom DNA Oligo
Gfi1b Forward: AGAAGGCTCACACCTACCAC		
Gfilb Reverse: GCTAGGCTTGTAGAATGGGGG	Integrated DNA Technologies	Custom DNA Oligo
Actb Forward: ACCTTCTACAATGAGCTGGG	Integrated DNA Technologies	Custom DNA Oligo
Actb Reverse: CCTGGATAGCAACGTACATGG	Integrated DNA Technologies	Custom DNA Oligo
Recombinant DNA		
MSCV-IRES-GFP	Addgene	CAT#20672; RRID: Addgene_20672
MSCV-IRES-mCherry	This paper	N/A
MSCV-IRES-mCherry-AML1-ETO-FKBP12^{F36V}-2xHA	This paper	N/A
MSCV-IRES-mCherry-AML1-ETO	This paper	N/A
MSCV-IRES-GFP-Gfi1b-FLAG	This paper	N/A
MSCV-IRES-GFP-AML1-ETO	This paper	N/A
MSCV-IRES-GFP-AML1-ETOΔNH1	This paper	N/A
MSCV-IRES-GFP-AML1-ETOΔNH2	This paper	N/A
MSCV-IRES-GFP-AML1-ETOΔNH3	This paper	N/A
MSCV-IRES-GFP-AML1-ETOΔNH4	This paper	N/A
MSCV-IRES-GFP-AML1-ETOΔNH4/NCOR	This paper	N/A
MSCV-IRES-GFP-AML1-ETO-R174Q	This paper	N/A
MSCV-IRES-GFP-AML1-ETO-F332A	This paper	N/A
MSCV-IRES-GFP-AML1-ETO-R668H	This paper	N/A
MSCV-IRES-GFP-AML1-ETO-G676C	This paper	N/A
MSCV-IRES-GFP-AML1-ETO-W692A	This paper	N/A
Software and Algorithms		
Bowtie2 (v. 2.2.2)	Langmead et al, 2012	N/A
MACS2 peak caller (narrowPeak; q-0.001; v. 2.0.10.20131216)	Feng et al., 2012	N/A

REAGENT or RESOURCE	SOURCE	IDENTIFIER
DiffBind	Ross-Innes et al., 2012	N/A
DESeq2	Love et al., 2014	N/A
HOMER	Heinz et al., 2010	N/A
deepTOOLS (v. 3.4.3)	Ramirez et al., 2016	N/A
FASTX toolkit (v. 0.0.13)	hannonlab.cshl.edu	N/A
TopHat (v. 2.0.11)	Trapnell et al., 2009	N/A
Cuffdiff (v. 2.1.1)	Trapnell et al., 2013	N/A
Nascent RNA Sequencing Anaylsis (NRSA)	Wang et al., 2018	N/A
Trimmomatic-0.32	Bolger et al., 2014	N/A
Other		
Alt-R® S.p. Cas9 Nuclease V3	Integrated DNA Technologies	CAT#1081059
CUTANA pAG-MNase for ChIC/CUT&RUN Workflows	Epicypher	CAT#15–1016